[redacted]

N70-34218

Copy No. 000

NASA Program Apollo Working Paper No. 1107

THE COMBINED EFFECT OF GRAVITY GRADIENT AND AERODYNAMIC TORQUES ON THE ATTITUDE CONTROL OF THE APOLLO/S-IVB IN A CIRCULAR ORBIT ABOUT THE EARTH

CASE FILE COPY

FOR NASA

DISTRIBUTION AND REFERENCING

This paper is not suitable for general distribution or referencing. It may be referenced only in other working correspondence and documents by participating organizations.

NATIONAL AERONAUTICS AND SPACE ADMINISTRATION
MANNED SPACECRAFT CENTER
Houston, Texas

February 14, 1964

NASA Program Apollo Working Paper No. 1107

THE COMBINED EFFECT OF GRAVITY GRADIENT AND AERODYNAMIC TORQUES ON THE ATTITUDE CONTROL OF THE APOLLO/S-IVB IN A CIRCULAR ORBIT ABOUT THE EARTH

Prepared by: Kenneth L. Lindsay

Kenneth L. Lindsay
AE, Control and Dynamics Section

AUTHORIZED FOR DISTRIBUTION:

Warren Gillespie, Jr.
for Maxime A. Faget
Assistant Director for Engineering and Development

NATIONAL AERONAUTICS AND SPACE ADMINISTRATION

MANNED SPACECRAFT CENTER

HOUSTON, TEXAS

February 14, 1964

TABLE OF CONTENTS

Section	Page
SUMMARY	1
INTRODUCTION	1
SYMBOLS	2
Subscripts	6
ANALYSIS	8
Equations of Motion	8
Inertial Attitude	9
Attitude Relative to Local Vertical	10
Coordinate Transformations	10
Aerodynamic Torque	12
Gravity Gradient Torque	17
Attitude Control System	17
TEST PROCEDURE	19
RESULTS AND DISCUSSION	22
PITCH COMMAND	22
Combined Pitch-Yaw Command	23
CONCLUDING REMARKS	24
REFERENCES	25
TABLES	26
FIGURES	28
APPENDIX A	36
APPENDIX B	53

LIST OF TABLES

Table		Page
I	Effect of Variation in Commanded Pitch Attitude on the Pitch-Axis Limit-Cycle Characteristics of the Apollo/S-IVB in a 100-Nautical-Mile Circular Earth Orbit	26
II	Effect of Variation in Specified Pitch Deadband on the Pitch-Axis Limit-Cycle Characteristics of the Apollo/S-IVB in a 100-Nautical-Mile Circular Earth Orbit	27

LIST OF FIGURES

Figure		Page
1	Block diagram of mathematical model	28
2	Coordinate systems utilized to analyze angular motions of Apollo/S-IVB in earth orbit	29
3	Configuration used to represent Apollo/S-IVB for aerodynamic computations	30
4	Euler angles defining attitude of vehicle relative to inertial space	31
5	Euler angles defining attitude of vehicle relative to local vertical	32
6	Orientation of resultant velocity and aerodynamic torque vectors relative to vehicle body axes	33
7	Disturbance torques acting on Apollo/S-IVB in a 100-nautical-mile circular orbit about the earth . . .	34
8	Comparison of desired and achieved pitch-axis phase plane trajectory of Apollo/S-IVB in a 100-nautical-mile circular orbit about the earth	35

THE COMBINED EFFECT OF GRAVITY GRADIENT AND AERODYNAMIC TORQUES ON THE ATTITUDE CONTROL OF THE APOLLO/S-IVB IN A CIRCULAR ORBIT ABOUT THE EARTH

SUMMARY

An analysis of the combined effect of aerodynamic and gravity gradient torques on the attitude control of the Apollo/S-IVB configuration during the earth-parking-orbit phase of a lunar landing mission is described. The parking orbit is assumed to be circular above the surface of a spherical earth of homogeneous mass distribution. Aerodynamic torques are determined by means of free-molecule impact theory, commonly referred to as specular reflection.

The equations utilized in the analysis were programed on the IBM 7094 computer using an assumed orbit altitude of 100 nautical miles. The effects of the disturbance torques on the limit-cycle characteristics of the vehicle were determined using the S-IVB attitude control system to maintain the vehicle at various pitch, yaw, and roll attitudes relative to the local horizontal within specified deadbands. Pure pitch attitudes (pitch axis normal to orbit plane, zero roll and yaw) of 0, 45, and 90 degrees relative to the local horizontal were simulated using specified deadbands varying from ±0.5 degrees to ±5 degrees. At all commanded attitudes, the vehicle damped to a steady-state limit cycle on one side of the pitch deadband instead of traversing the entire deadband as desired. The frequencies of these limit cycles were considerably higher than those which would exist in the absence of disturbing torques, resulting in increased control system fuel consumption.

A combined maneuver in which the vehicle was commanded to maintain simultaneously a pitch and yaw attitude relative to the local horizontal of 30 degrees each within a ±5 degree specified deadband about each axis was also simulated. The limit-cycles about both the pitch and yaw axes exhibited a similar behavior to the pure pitch command described above, although the amplitudes and frequencies were different in pitch from those in yaw.

INTRODUCTION

A satellite in earth orbit is acted upon by numerous environmental disturbance torques which affect its angular motion. These include torques resulting from gravity gradient, solar pressure, electric and magnetic fields, meteorites, and aerodynamics. Rough estimates given by

Roberson in reference 1 indicate that the most significant of these torques for a low-altitude orbit result from gravity gradient and aerodynamics. The effect of gravity gradient on the angular motions of an earth satellite has been analyzed by various authors such as Doolin (ref. 2). The effect of aerodynamics on the angular motions of certain satellite configurations at low altitudes has been studied by DeBra (ref. 3).

The present study investigates the combined effect of gravity gradient and aerodynamics on the attitude control of the Apollo/S-IVB in a circular orbit about the earth. According to present plans, the Apollo/S-IVB configuration will be maintained at some specified attitude relative to the local vertical within predetermined deadbands in pitch, yaw, and roll by means of reaction jets during the earth orbital phase of the lunar landing mission. This requirement arises from the need to orient communications equipment on board the vehicle to earth-based flight monitors, as well as to orient an onboard sextant for star and landmark sightings to establish vehicle position. The S-IVB control system will be the primary means of attitude control and the Apollo service module control system may be used as a backup.

The mathematical model employed to analyze the combined effect of aerodynamic and gravity gradient torques on the attitude control of the vehicle, as well as results obtained using the S-IVB attitude control system to maintain various attitudes relative to the local vertical, is herein presented.

The author wishes to acknowledge the assistance of Mr. James L. Long of the Computation and Data Reduction Division, NASA Manned Spacecraft Center, who programed and checked the digital computer mechanization of the equations used in this study.

SYMBOLS

A	Length of cone removed to form cone frustum (fig. A-4), ft
a	Distance from vehicle center of mass to elemental mass in vehicle, ft
C	Aerodynamic force component along x-axis, lb
C_N	Normal force coefficient, dimensionless

C_1, C_2, C_3	Constants used to determine control torque direction about the x-, y-, and z-axes, respectively, (equations 60 to 65), dimensionless
D	Diameter of cylinder used to represent Saturn S-IVB booster, ft
D_1	Diameter of cylinder used to represent service module plus LEM shroud
d	Differential operator, dimensionless
l_C	Cone center of pressure distance from apex along x-axis, ft
l_{CM}	Command module center of pressure distance from nose along x-axis, ft
$l_{c.p.}$	Combined center of pressure distance from combined center of mass along x-axis, ft
l_{cyl}	Cylinder center of pressure distance from front along x-axis, ft
l_F	Cone frustum center of pressure distance from small end along x-axis, ft
l_L	Large cone center of pressure location used to determine cone frustum center of pressure location (appendix A), ft
l_S	Small cone center of pressure used to determine cone frustum center of pressure (appendix A), ft
$l_{SM/LEM}$	Service module plus lunar excursion module shroud center of pressure distance from front of service module along x-axis, ft
l_{S-IVB}	Saturn S-IVB center of pressure distance from front along x-axis, ft
M	Resultant torque acting on vehicle, ft-lb
M_{x_J}, M_{y_J}, M_{z_J}	Control torque about x-, y-, and z-axes, respectively, ft-lb
M_1, M_2, M_3	Magnitude of control torque about x-, y-, and z-axes, respectively, ft-lb

m	Mass of vehicle, slugs
N	Aerodynamic normal force acting on vehicle, lb
$\hat{P}$	Unit vector perpendicular to an elemental area on surface of vehicle, dimensionless
q	Dynamic pressure, lb/ft^2
$\overline{R}$	Vector distance from earth center of mass to vehicle center of mass, ft
r	Radius of cone intermediate cross-section (fig. A-3), ft
r_{cyl}	Radius of cylinder cross-section (fig. A-5)
$\overline{r}_m$	Vector distance from earth center of mass to elemental mass in vehicle, ft
S	Cross-sectional area of S-IVB, $\pi D^2/4$, ft^2
T_1	Orthogonal matrix transformation from the x_o, y_o, and z_o-axis system to the x, y, and z-axis system, dimensionless
t	time, sec
$\overline{V}$	Velocity of vehicle relative to the atmosphere (equal to inertial velocity in present analysis), ft/sec
x, y, z	Vehicle body axes having origin at combined center of mass with x-axis positive forward through command module nose, y- and z-axes completing right-handed system
x_c, y_c, z_c	Cone body axes having origin at apex with x_c-axis positive rearward, y_c- and z_c-axes completing right-handed system (fig. A-2)
x'_c, y'_c, z'_c	Axes parallel to x_c- and z_c-axes, respectively, with origin at center of elemental area on surface of cone (fig. A-2)

$X_{c.m.}$	Distance along x-axis from nose of command module to vehicle combined center of mass, ft
$X_{c.p.}$	Distance along x-axis from nose of command module to vehicle combined center of pressure, ft
x_{cyl}, y_{cyl}, z_{cyl}	Cylinder body axes having origin at end with x_{cyl}-axis positive rearward, y_{cyl}- and z_{cyl}-axes completing right-handed system (fig. A-5)
x_o, y_o, z_o	Inertial cartesian axis system having origin at center of spherical earth with y_o-axis normal to orbit plane, x_o- and z_o-axes completing right-handed system (fig. 2)
x_r, y_r, z_r	Cartesian coordinate system having origin at center of spherical earth with x_r-axis parallel to local horizontal (positive in direction of motion) y_r-axis normal to orbit plane and z_r-axis along $\overline{R}$ (positive outward from center of earth)
α	Combined angle of attack, or angle between x-axis and $\overline{V}$, degrees
β_1	Angle in y_c z_c-plane between y_c-axis and line from x_c-axis to projection on y_c z_c-plane of point on surface of cone (fig. A-2), degrees
β_{1_u}	Values of β_1 corresponding to points on line along cone surface separating portion of surface exposed to air flow from portion shielded from air flow, degrees
β_2	Angle related to cone frustum corresponding to β_1 for cone, degrees
β_{2_u}	Angle related to cone frustum corresponding to β_{1_u} for cone, degrees
β_{3_u}	Angle related to cylinder corresponding to β_{1_u} for cone, degrees
Γ	$\dot{\Gamma}_o t$, Angle in orbit plane between z_o-axis and z_r-axis, degrees

$\dot{\Gamma}$	Constant orbital angular rate, or angular rate of x_r-, y_r-, and z_r-axes relative to x_o-, y_o-, and z_o-axes, rad/sec
δ_1	Semi-apex angle of cone used to represent command module, degrees
δ_2	Semi-apex angle of cone frustum used to represent adapter between LEM shroud and S-IVB, degrees
ϵ	Angle between $\overline{V}$ and line of intersection between cone surface and plane containing $\overline{V}$ and x_c-axis (fig. A-1), degrees
η	Angle between $\overline{V}$ and line normal to cone surface in plane containing $\overline{V}$ and x_c-axis (fig. A-1), degrees
θ, ψ, ϕ	Euler angles defining orientation of xyz-triad relative to $x_o y_o z_o$-triad, degrees
θ_r, Ψ_r, ϕ_r	Euler angles defining orientation of xyz-triad relative to $x_r y_r z_r$-triad, degrees
θ_{r_c}, Ψ_{r_c}, ϕ_{r_c}	Commanded values of θ_r, Ψ_r, and ϕ_r, respectively, degrees
ρ	Atmospheric density, slugs/ft^3
τ_x, τ_y, τ_z	Width (duration) of attitude control jet pulses about x-, y-, and z-axes, respectively, seconds
τ_{x_1}, τ_{y_1}, τ_{z_1}	Time between attitude control jet pulses about x-, y-, and z-axes, respectively, seconds
ϕ_b	Aerodynamic roll-angle, or angle between $\overline{M}_a$ and y-axis in yz-plane, degrees
Ω	Resultant angular rate of vehicle in inertial space, rad/sec

Subscripts

A	Adapter between service module plus LEM shroud and S-IVB

a	Aerodynamic
C	Cone
E_x, E_y, E_z	Error functions used to command control torques about the x-, y-, and z-axes, respectively, dimensionless
F	Resultant aerodynamic force acting on vehicle, lb
F_G	Inverse-square-law gravitational force acting on vehicle due to earth, lb
H_{x_1}, H_{y_1}, H_{z_1}	Lower (negative) deadbands about the x-, y-, and z-axes respectively, radians
H_{x_2}, H_{y_2}, H_{z_2}	Upper (positive) deadbands about the x-, y-, and z-axes, respectively, radians
I_x, I_y, I_z	Moments of inertia about the x-, y-, and z-axes, respectively, slug-ft^2
$\hat{i}$, $\hat{j}$, $\hat{k}$	Unit vectors along the x-, y-, and z-axes, respectively, dimensionless
$\hat{i}_c$, $\hat{j}_c$, $\hat{k}_c$	Unit vectors along the x_c-, y_c-, and z_c-axes, respectively
K	Geocentric gravitational constant of the earth, 1.407656×10^{16} ft^3/sec^2
K_1, K_3, K_5	Rate gains in attitude control system, rad/rad/sec
K_2, K_4, K_6	Attitude gains in attitude control system, rad/rad
L	Length of cylinder used to represent S-IVB booster, ft
L_1	Length of cone used to represent command module, ft
L_2	Length of cylinder used to represent service module plus LEM shroud, ft
L_3	Length of cone frustum used to represent adapter between the service module plus LEM shroud and the S-IVB booster, ft

l_A	Adapter center of pressure distance from front along x-axis, ft
CM	Command module
cyl	Cylinder
f	Cone frustum
G	Gravity gradient
L	Large cone
S	Small cone
SM/LEM	Service module plus lunar excursion module shroud
S-IVB	Saturn booster used for translunar orbit injection
T	Total or resultant
x, y, z	Components along x-, y-, and z-axes, respectively
x_o, y_o, z_o	Components along x_o-, y_o-, and z_o-axes, respectively

In addition, a $(\dot{\ })$ over a symbol represents a derivative with respect to time and a $(\bar{\ })$ over a symbol represents a vector.

ANALYSIS

Equations of Motion

The mathematical model employed for this investigation was a rigid vehicle moving in a circular orbit about a spherical, homogeneous, nonrotating earth. A block diagram of the mathematical model is shown in figure 1. The coordinate systems used are shown in figure 2 and the geometry of the vehicle is shown in figure 3. The body axes of the vehicle are assumed to be principal axes and the moments of inertia of the vehicle are assumed to be constant. Under these conditions, the rotational equations of motion are, from reference 4,

$$\dot{\Omega}_x = \left[M_{x_G} + M_{x_J} - \Omega_y \Omega_z (I_z - I_y)\right] / I_x \tag{1}$$

$$\dot{\Omega}_y = \left[M_{y_a} + M_{y_G} + M_{y_J} - \Omega_x \Omega_z (I_x - I_z)\right] / I_y \tag{2}$$

$$\dot{\Omega}_z = \left[M_{z_a} + M_{z_G} + M_{z_J} - \Omega_x \Omega_y (I_y - I_x)\right] / I_z \tag{3}$$

The effect of attitude control jet and aerodynamic forces on the orbit parameters are assumed to be negligible for the length of time during which the vehicle remains in earth orbit, that is, the velocity and altitude of the vehicle are constrained to remain constant, the plane of the orbit being fixed in inertial space. Consequently, the translational equations of motion are not included in this study.

Inertial Attitude

The attitude of the vehicle relative to inertial space can be determined by use of Euler angles. From figure 4, the components of angular velocity about the body axes in terms of Euler angles and Euler angular rates are seen to be

$$\Omega_x = \dot{\phi} + \dot{\theta} \sin \psi \tag{4}$$

$$\Omega_y = \dot{\psi} \sin \phi + \dot{\theta} \cos \psi \cos \phi \tag{5}$$

$$\Omega_z = \dot{\psi} \cos \phi - \dot{\theta} \cos \psi \sin \phi \tag{6}$$

Solving equations (4), (5), and (6) simultaneously to obtain the Euler angular rates,

$$\dot{\phi} = \Omega_x - \dot{\theta} \sin \psi \tag{7}$$

$$\dot{\psi} = \Omega_y \sin \phi + \Omega_z \cos \phi \tag{8}$$

$$\dot{\theta} = \left[\Omega_y \cos \phi - \Omega_z \sin \phi\right] / \cos \psi \tag{9}$$

Equations (7), (8), and (9) can then be integrated numerically with respect to time to obtain the attitude of the vehicle relative to inertial

space, that is, the orientation of the xyz-triad relative to the $x_o y_o z_o$-triad.

Attitude Relative to Local Vertical

The attitude of the vehicle relative to the local vertical can be determined by use of Euler angles by superimposing a fourth angle to represent the rotation of the local vertical relative to inertial space, as shown in figure 5. As can be seen from figure 5,

$$\Omega_x = (\dot{\Gamma} + \dot{\theta}_r) \sin \psi_r + \dot{\phi}_r \tag{10}$$

$$\Omega_y = (\dot{\Gamma} + \dot{\theta}_r) \cos \psi_r \cos \phi_r + \dot{\psi}_r \sin \phi_r \tag{11}$$

$$\Omega_z = \dot{\psi}_r \cos \phi_r - (\dot{\Gamma} + \theta_r) \cos \psi_r \sin \phi_r \tag{12}$$

Solving equations (10), (11), and (12) simultaneously to obtain the relative Euler angular rates,

$$\dot{\phi}_r = \Omega_x - (\dot{\Gamma} + \dot{\theta}_r) \sin \psi_r \tag{13}$$

$$\dot{\psi}_r = \Omega_y \sin \phi_r + \Omega_z \cos \phi_r \tag{14}$$

$$\dot{\theta}_r = \left[\Omega_y \cos \phi_r - \Omega_z \sin \phi_r - \dot{\Gamma} \cos \psi_r\right] \Big/ \cos \psi_r \tag{15}$$

Equations (13), (14), and (15) can then be integrated numerically with respect to time to obtain the attitude of the vehicle relative to the local vertical, that is, the orientation of the xyz-triad relative to the $x_r y_r z_r$-triad.

Coordinate Transformations

The components of vehicle position and velocity along the x_o-, y_o-, and z_o-axes are, from figure 2,

$$R_{x_o} = R \sin \Gamma \tag{16}$$

$$R_{y_o} = 0 \tag{17}$$

$$R_{z_o} = R \cos \Gamma \tag{18}$$

and

$$V_{x_o} = V \cos \Gamma \tag{19}$$

$$V_{y_o} = 0 \tag{20}$$

$$V_{z_o} = -V \sin \Gamma \tag{21}$$

The components of orbital angular rate along the x_o-, y_o-, and z_o-axes are, from figure 5,

$$\dot{\Gamma}_{x_o} = 0 \tag{22}$$

$$\dot{\Gamma}_{y_o} = \dot{\Gamma} \tag{23}$$

$$\dot{\Gamma}_{z_o} = 0 \tag{24}$$

The matrix transformation from the $x_o y_o z_o$-triad to the xyz-triad is, from figure 4,

$$\left[T_1\right] = \begin{bmatrix} (\cos \psi \cos \theta) & (\sin \psi) & (-\sin \theta \cos \psi) \\ (\sin \phi \sin \theta & (\cos \phi \cos \psi) & (\sin \theta \sin \psi \cos \phi \\ - \sin \psi \cos \theta \cos \phi) & & + \sin \phi \cos \theta) \\ (\sin \psi \cos \theta \sin \phi & (-\sin \phi \cos \psi) & (\cos \phi \cos \theta \\ + \sin \theta \cos \phi) & & -\sin \phi \sin \theta \sin \psi) \end{bmatrix} \tag{25}$$

The components of vehicle position and velocity along the x-, y-, and z-axes are then

$$\begin{bmatrix} R_x \\ R_y \\ R_z \end{bmatrix} = \begin{bmatrix} T_1 \end{bmatrix} \begin{bmatrix} R_{x_o} \\ R_{y_o} \\ R_{z_o} \end{bmatrix} \tag{26}$$

and

$$\begin{bmatrix} V_x \\ V_y \\ V_z \end{bmatrix} = \begin{bmatrix} T_1 \end{bmatrix} \begin{bmatrix} V_{x_o} \\ V_{y_o} \\ V_{z_o} \end{bmatrix} \tag{27}$$

The components of orbital angular rate along the xyz-axes are

$$\begin{bmatrix} \dot{\Gamma}_x \\ \dot{\Gamma}_y \\ \dot{\Gamma}_z \end{bmatrix} = \begin{bmatrix} T_1 \end{bmatrix} \begin{bmatrix} \dot{\Gamma}_{x_o} \\ \dot{\Gamma}_{y_o} \\ \dot{\Gamma}_{z_o} \end{bmatrix} \tag{28}$$

Aerodynamic Torque

The configuration shown in figure 3 is assumed to represent the Apollo/S-IVB for the purpose of aerodynamic calculations.

As shown, the command module is represented by a right circular cone, the service module/LEM shroud and Saturn S-IVB by right circular cylinders and the S-IVB adapter by a right circular cone frustum.

The total normal force coefficient for this configuration is determined by summing the normal force coefficients of the individual components, that is,

$$C_{N_T} = C_{N_{CM}} + C_{N_{SM/LEM}} + C_{N_A} + C_{N_{S-IVB}} \tag{29}$$

where all coefficients are based on a common reference area and shielding of various components by upstream components are assumed to be negligible. The coefficients for the individual components are derived in Appendix A. The resulting expressions are listed below, each based on the cross-sectional area of the S-IVB, $\pi D^2/4$. For the command module,

$$C_{N_{CM}} = 2\left(\frac{D_1}{D}\right)^2 \cos^2 \delta_1 \sin 2\alpha \qquad \text{when } \alpha \leq \delta_1 \tag{30}$$

$$\begin{aligned} C_{N_{CM}} = \frac{2}{\pi}\left(\frac{D_1}{D}\right)^2 \cot \delta_1 \Bigg\{ & \frac{1}{2}\left(\beta_{1_u} + \frac{\pi}{2}\right) \sin 2\alpha \sin 2\delta_1 \\ & + \cos \beta_{1_u} \Bigg[2 \cos^2 \alpha \sin^2 \delta_1 - \frac{1}{2} \sin 2\alpha \sin 2\delta_1 \sin \beta_{1_u} \\ & + \frac{2}{3} \sin^2 \alpha \cos^2 \delta_1 \left(\sin^2 \beta_{1_u} + 2\right)\Bigg]\Bigg\} \quad \text{when } \alpha > \delta_1 \end{aligned} \tag{31}$$

where, from figure 6,

$$\alpha = \tan^{-1} \frac{\sqrt{V_y^2 + V_z^2}}{V_x} \tag{32}$$

and, from Appendix A,

$$\beta_{1_u} = \cos^{-1} \frac{\sqrt{\tan^2\alpha - \tan^2\delta_1}}{\tan \alpha} \tag{33}$$

For the service module/LEM shroud,

$$C_{N_{SM/LEM}} = \frac{32}{3\pi} \frac{L_2 D_1}{D^2} \sin^2 \alpha \tag{34}$$

For the S-IVB adapter,

$$C_{N_A} = 2\left[1 - \left(D_1/D\right)^2\right] \cos^2 \delta_2 \sin 2\alpha \quad \text{when } \alpha \leq \delta_2 \tag{35}$$

$$C_{N_A} = \frac{2}{\pi} \cot \delta_2 \left[1 - \left(D_1/D\right)^2\right] \left\{\frac{1}{2}\left(B_{2_u} + \frac{\pi}{2}\right) \sin 2\alpha \sin 2\delta_2 \right.$$

$$+ \cos \beta_{2_u} \left[2 \cos^2\alpha \sin^2 \delta_2 - \frac{1}{2} \sin 2\alpha \sin 2\delta_2 \sin \beta_{2_u}\right.$$

$$\left.\left. + \frac{2}{3} \sin^2 \alpha \cos^2 \delta_2 \left(\sin^2 \beta_{2_u} + 2\right)\right]\right\} \quad \text{when } \alpha > \delta_2 \tag{36}$$

where, replacing β_{1_u} and δ_1 by β_{2_u} and δ_2 respectively, in equation (33),

$$\beta_{2_u} = \cos^{-1} \frac{\sqrt{\tan^2\alpha - \tan^2\delta_2}}{\tan \alpha} \tag{37}$$

For the Saturn S-IVB,

$$C_{N_{S\text{-}IVB}} = \frac{32}{3\pi}\left(\frac{L}{D}\right) \sin^2\alpha \tag{38}$$

From figure 3, the resultant aerodynamic moment about the nose of the command module,

$$M_{a_{NOSE}} = q\pi \frac{D^2}{4} \left[C_{N_{CM}} l_{CM} + C_{N_{SM/LEM}} \left(L_1 + l_{SM/LEM}\right)\right.$$

$$\left. + C_{N_A} \left(L_1 + L_2 + l_A\right) + C_{N_{S\text{-}IVB}} \left(L_1 + L_2 + L_3 + l_{S\text{-}IVB}\right)\right] \tag{39}$$

But, from Appendix A,

$$l_{CM} = \frac{2}{3} L_1 \tag{40}$$

$$l_{SM/LEM} = \frac{1}{2} L_2 \tag{41}$$

$$l_A = \frac{L_3(D_1 + 2D)}{3\,(D_1 + D)} \tag{42}$$

$$l_{S-IVB} = \frac{1}{2} L \tag{43}$$

Substituting equations (40) through (43) into equation (39) and simplifying,

$$\begin{aligned} M_{a_{NOSE}} = q\,\frac{\pi D^2}{4} \Bigg\{ & L_1 \left[(2/3)\ C_{N_{CM}} + C_{N_{SM/LEM}} + C_{N_A} + C_{N_{S-IVB}} \right] \\ & + L_2 \left[(1/2)\ C_{N_{SM/LEM}} + C_{N_A} + C_{N_{S-IVB}} \right] + (1/2)\ L\ C_{N_{S-IVB}} \\ & + L_3 \left[(D_1 + 2D)\ C_{n_A} / 3\ (D_1 + D) + C_{N_{S-IVB}} \right] \Bigg\} \end{aligned} \tag{44}$$

The resultant normal force on the vehicle

$$N_T = C_{N_T}\ q\pi D^2/4 \tag{45}$$

The distance of the resultant center of pressure from the nose of the command module is then determined by the ratio of resultant moment about the nose to resultant normal force, that is,

$$X_{c.p.} = M_{a_{NOSE}} / N_T \tag{46}$$

Substituting equations (44) and (45) into equation (46) and reducing,

$$X_{c.p.} = \left\{ L_1 \left[(2/3)\ C_{N_{CM}} + C_{N_{SM/LEM}} + C_{N_A} + C_{N_{S-IVB}} \right] \right.$$

$$+ L_2 \left[(1/2)\ C_{N_{SM/LEM}} + C_{N_A} + C_{N_{S-IVB}} \right] + (1/2)\ LC_{N_{S-IVB}}$$

$$\left. + L_3 \left[(D_1 + 2D)\ C_{N_A} / 3\ (D_1 + D) + C_{N_{S-IVB}} \right] \right\} \Big/ C_{N_T} \qquad (47)$$

The distance of the resultant center of pressure from the resultant center of mass

$$l_{c.p.} = X_{c.m.} - X_{c.p.} \qquad (48)$$

The resultant aerodynamic moment about the center of mass

$$M_a = C_{N_T}\ qS\ l_{c.p.} \qquad (49)$$

and acts about an axis normal to the plane containing the x-axis and the resultant velocity vector, as shown in figure 6. The components about each of the body axes are

$$M_{x_a} = 0 \qquad (50)$$

$$M_{y_a} = M_a \cos \phi_b \qquad (51)$$

$$M_{z_a} = M_a \sin \phi_b \qquad (52)$$

where, from figure 6,

$$\phi_b = \tan^{-1} \left(\frac{V_y}{V_z} \right) \qquad (53)$$

Gravity Gradient Torque

The torque produced by gravity gradient on a vehicle in an inverse-square force field is treated in Appendix B. Expressions are developed to determine the components of this torque about an arbitrary set of orthogonal body axes of an arbitrary vehicle. Since the body axes of the Apollo/S-IVB are assumed to be principal axes in the present analysis, the components of gravity gradient torque about these axes are (see Appendix B),

$$M_{x_G} = \frac{3K}{R^5} R_y R_z (I_z - I_y) \tag{54}$$

$$M_{y_G} = \frac{3K}{R^5} R_x R_z (I_x - I_z) \tag{55}$$

$$M_{z_G} = \frac{3K}{R^5} R_x R_y (I_y - I_x) \tag{56}$$

Attitude Control System

The attitude control system employed in the present analysis consists of constant magnitude jets mounted on the vehicle to produce torque about each of the body axes.

The jets producing control torque about each of the body axes are fired at constant frequency and constant width (duration) as commanded by the control logic for each axis. The system is assumed to be ideal, that is, the pulses are rectangular and no hysteresis or time delays exist.

The error signals used to command control torques about the x-, y-, and z-axes respectively are:

$$E_x = K_1 (\Omega_x - \dot{\Gamma}_x) + K_2 (\phi_r - \phi_{r_c}) \tag{57}$$

$$E_y = K_3 (\Omega_y - \dot{\Gamma}_y) + K_4 (\theta_r - \theta_{r_c}) \tag{58}$$

$$E_z = K_5 (\Omega_z - \dot{\Gamma}_z) + K_6 (\psi_r - \psi_{r_c}) \tag{59}$$

The quantities $\dot{\Gamma}_x$, $\dot{\Gamma}_y$, and $\dot{\Gamma}_z$ in equations (57), (58), and (59), respectively, remove the angular rate of the $x_r y_r z_r$-triad relative to inertial space so that the error functions E_x, E_y, and E_z are analogous to a familiar inertial attitude command system rate feedback.

The control torques about the x-, y-, and z-axes, respectively, are:

$$M_{x_J} = C_1 M_1 \tag{60}$$

$$M_{y_J} = C_2 M_2 \tag{61}$$

$$M_{z_J} = C_3 M_3 \tag{62}$$

where

$$C_1 = \left\{ \begin{array}{l} 1 \text{ for } \tau_x \text{ seconds, then } 0 \text{ for } \tau_{x_1} \text{ seconds} \\ \text{and repeat if } E_x < H_{x_1} \\ -1 \text{ for } \tau_x \text{ seconds, then } 0 \text{ for } \tau_{x_1} \text{ seconds, and repeat if} \\ E_x > H_{x_2} \\ 0 \text{ if } H_{x_1} \leq E_x \leq H_{x_2} \end{array} \right\} \tag{63}$$

$$C_2 = \left\{ \begin{array}{l} 1 \text{ for } \tau_y \text{ seconds, then } 0 \text{ for } \tau_{y_1} \text{ seconds, and repeat} \\ \text{if } E_y < H_{y_1} \\ -1 \text{ for } \tau_y \text{ seconds, then } 0 \text{ for } \tau_{y_1} \text{ seconds, and repeat if} \\ E_y > H_{y_2} \\ 0 \text{ if } H_{y_1} \leq H_{y_2} \end{array} \right\} \tag{64}$$

$$C_3 = \begin{cases} 1 \text{ for } \tau_z \text{ seconds, then } 0 \text{ for } \tau_{z_1} \text{ seconds, and repeat} \\ \text{if } E_z < H_{z_1} \\ -1 \text{ for } \tau_z \text{ seconds, then } 0 \text{ for } \tau_{z_1} \text{ seconds, and repeat} \\ \text{if } E_z > H_{z_2} \\ 0 \text{ if } H_{z_1} \leq E_z \leq H_{z_2} \end{cases} \quad (65)$$

TEST PROCEDURE

All attitude command maneuvers simulated corresponded to a circular orbit at an altitude of 100 nautical miles above the surface of the earth. The vehicle and orbital parameters for all maneuvers were:

$A = 18.833$ ft

$D = 21.667$ ft

$D_1 = 12.833$ ft

$I_x = 8.62 \times 10^4$ slug-ft^2

$I_y = 9.75 \times 10^6$ slug-ft^2

$I_z = 9.75 \times 10^6$ slug-ft^2

$K = 1.4075 \times 10^{16}$ ft^3/sec^2

$K_1 = K_3 = K_5 = 5$ rad/rad/sec

$K_2 = K_4 = K_6 = 1$ rad/rad

$L = 43.625$ ft

$L_1 = 11.583$ ft

$L_2 = 32.700$ ft

$L_3 = 12.917$ ft

$M_1 = 3.489 \times 10^3$ ft-lb

$M_2 = 3.702 \times 10^3$ ft-lb

$M_3 = 8.476 \times 10^3$ ft-lb

$\bar{R} = 2.15115 \times 10^7$ ft

$\bar{V} = 2.5579 \times 10^4$ ft/sec

$X_{c.m.} = 73.10$ ft

$\bar{\dot{\Gamma}} = 6.812468 \times 10^{-2}$ deg/sec

$\delta_1 = 33.06$ deg

$\delta_2 = 18.85$ deg

$\rho = 9.67 \times 10^{-13}$ slugs/ft^3

$\tau_x = \tau_y = \tau_z = 0.05$ seconds

$\tau_{x_1} = \tau_{y_1} = \tau_{z_1} = 0.95$ seconds

A series of pitch command maneuvers were simulated requiring the initial conditions listed below:

$\psi = 0$

$\phi = 0$

$\psi_r = 0$

$\phi_r = 0$

$\psi_{r_c} = 0$

$$\phi_{r_c} = 0$$

$$\Omega_x = 0$$

$$\Omega_y = \dot{\Gamma} = 6.812468 \times 10^{-2} \text{ deg/sec}$$

$$\Omega_z = 0$$

$$\Gamma = 0$$

Commanded pitch attitudes (θ_{r_c}) of 0, 45, and 90 degrees were simulated. At each attitude, results were obtained for desired deadbands ranging from ± 0.5 degrees to ± 5 degrees.

A combined pitch and yaw maneuver was simulated wherein the initial conditions listed above were applicable with the following changes:

$$H_{x_1} = H_{y_1} = H_{z_1} = -5 \text{ deg}$$

$$H_{x_2} = H_{y_2} = H_{z_2} = 5 \text{ deg}$$

$$\theta = 35 \text{ deg}$$

$$\psi = 35 \text{ deg}$$

$$\phi = 0 \text{ deg}$$

$$\theta_r = 35 \text{ deg}$$

$$\psi_r = 35 \text{ deg}$$

$$\phi_r = 0 \text{ deg}$$

$$\theta_{r_c} = 30 \text{ deg}$$

$$\psi_{r_c} = 30 \text{ deg}$$

$$\phi_{r_c} = 0$$

$$\Omega_x = \dot{\Gamma}_x = 0.03907 \text{ deg/sec}$$

$$\Omega_y = \dot{\Gamma}_y = 0.04571 \text{ deg/sec}$$

$$\Omega_z = \dot{\Gamma}_z = 0.03201 \text{ deg/sec}$$

Each of the above maneuvers was simulated for a time sufficient to allow the limit-cycle periods about each axis to damp to steady-state values.

RESULTS AND DISCUSSION

A series of maneuvers using the Saturn S-IVB attitude control system to maintain the Apollo/S-IVB at different pitch attitudes relative to the local horizontal was simulated. The vehicle was initially oriented with the y-axis normal to the orbit plane; consequently, the resultant aerodynamic and gravity torques acted about that axis, the x- and z-axes being unaffected. In addition, a combined maneuver in which the vehicle was commanded to maintain simultaneously a pitch and yaw attitude relative to the local horizontal, a situation which could be required for a navitation sighting or other operation, was also simulated.

PITCH COMMAND

The vehicle damped to a steady-state limit cycle on one side of the specified pitch deadband instead of traversing the entire deadband at each commanded pitch attitude. This behavior is a consequence of the unidirectional disturbance torques (fig. 7) acting about the y-axis tending to increase the pitch attitude. As an example of this behavior, consider the case listed in table I for a commanded pitch attitude of 0 degrees with a specified deadband of ± 0.5 degrees. As shown in figure 8, when the vehicle reaches the +0.5-degree side of the deadband from within the deadband at a sufficiently low rate, the pitch attitude control jet will impart a minimum impulse to the vehicle and reverse the direction of rotation. The disturbance torques are then acting in a direction opposite to the direction of rotation with sufficient magnitude to stop the rotation before the vehicle reaches the -0.5-degree side of the deadband and force it to start back toward the +0.5-degree side of the deadband. This behavior continues until a steady-state condition is reached wherein

the vehicle rotates 0.053 degrees away from the +0.5-degree side of the deadband in the direction of the -0.5-degree side, reverses direction and returns, the cycle repeating (and the jet firing) every 413 seconds. Similar results were obtained at the other commanded attitudes examined, as shown in table I.

The resulting limit-cycle widths and periods were found to vary with specified deadband width at the commanded attitudes examined. This variation came about because the vehicle always remained in close proximity to one side of the specified deadband, thus subjecting the vehicle to varying (attitude-dependent) disturbance torques. This variation is seen from table I to be especially significant for a commanded pitch attitude of 0 degrees, the resulting limit-cycle period varying from 413 seconds for a ±0.5 degree-specified deadband to 33 seconds for a ±5-degree specified deadband. For this reason, a series of maneuvers were simulated wherein the commanded pitch attitude was 0 degrees and the specified deadband widths were varied from ±0.5 degrees to ±5 degrees in increments of 0.5 degrees. Both the deadband widths and limit-cycle periods resulting decreased as the specified deadband widths increased. The results obtained are summarized in table II.

Combined Pitch-Yaw Command

The pitch and yaw attitudes were each commanded to 30 degrees within a ±5-degree deadband. The limit-cycles about both the pitch and yaw axes exhibited similar behavior to the pure pitch command described above. The pitch deadband width obtained was 0.001 degrees with a period of 7 seconds at the +5-degree side of the deadband. The yaw deadband width obtained was 0.008 degrees with a period of 54 seconds at the -5-degree side of the deadband. The difference in limit-cycle characteristics in pitch and yaw was due in part to the gravity gradient and aerodynamic torques being in the same direction (positive) in pitch, but in opposite directions in yaw. Another source of difference was the inertia cross-coupling between the pitch and yaw axes through the roll axis because a roll rate was required as a component of the orbital angular rate (rotation rate of local horizontal in the orbit plane). Although this cross-coupling was insignificant compared to the gravity gradient and aerodynamic torques about the pitch axis, it dominated the motion about the yaw axis. The final difference arose because the control torque about the yaw axis was greater than the control torque about the pitch axis (two 150-pound-thrust jets produce torque in either direction for yaw control, whereas only one 150-pound-thrust jet is available for pitch control in each direction), while the moments of inertia in pitch and yaw were equal.

CONCLUDING REMARKS

Gravity gradient and aerodynamic torques acting on the Apollo/S-IVB in a 100-nautical-mile circular orbit about the earth are of sufficient magnitude to have a significant deleterious effect on the limit-cycle operation of the Saturn S-IVB attitude control system about both the pitch and yaw axes of the vehicle. At the commanded attitudes considered in the present analysis, the torques forced the vehicle to damp to a steady-state limit-cycle on one side of the pitch and yaw specified deadbands instead of traversing the entire deadbands, resulting in frequencies considerably higher than the no-disturbance-torque condition.

At commanded attitudes near zero, the frequency of the steady-state limit-cycles about the pitch or yaw axis can be considerably reduced by decreasing the specified deadbands, resulting in a decrease in attitude control fuel consumption. At larger commanded attitudes, the effect of varying the specified deadbands is less pronounced.

REFERENCES

1. Roberson, Robert E.: Attitude Control of a Satellite Vehicle – An Outline of the Problems. Presented at the Eighth International Astronautical Congress, Barcelona, Spain, ARS Paper 485-57, Oct. 1957.

2. Doolin, Brian F.: Gravity Torque on an Orbiting Vehicle. NASA TN D-70, 1959.

3. DeBra, D. B.: The Effect of Aerodynamic Forces on Satellite Attitude. Advances in Astronautical Sciences, vol. 3.

4. MacMillan, William Duncan: Dynamics of Rigid Bodies. 2nd ed., Dover Publications, Inc., New York 14, New York, 1960, pp. 183-184.

5. Truitt, Robert Wesley: Hypersonic Aerodynamics. The Ronald Press Company, New York, 1959, pp. 6, 71-88, and 154.

6. Thomson, William Tyrrell: Introduction to Space Dynamics. John Wiley and Sons, Inc., New York, 1961, pp. 94-97, and 146-147.

TABLE I.- EFFECT OF VARIATION IN COMMANDED PITCH ATTITUDE ON THE PITCH-AXIS LIMIT-CYCLE CHARACTERISTICS OF THE APOLLO/S-IVB IN A 100-NAUTICAL-MILE CIRCULAR EARTH ORBIT*

Commanded pitch attitude (degrees)	Specified deadband width (degrees)	Resulting deadband width (degrees)	Resulting limit cycle period (sec)
0	±5	.003	33
45	±5	.001	5
90	±5	.002	14
0	±0.5	.053	413
45	±0.5	.001	6
90	±0.5	.001	11

*S-IVB attitude control system with minimum pulse duration of 50ms and 150-pound-thrust jets used.

TABLE II.- EFFECT OF VARIATION IN SPECIFIED PITCH DEADBAND ON THE PITCH-AXIS LIMIT-CYCLE CHARACTERISTICS OF THE APOLLO/S-IVB IN A 100-NAUTICAL-MILE CIRCULAR EARTH ORBIT*

Commanded pitch attitude (degrees)	Specified deadband width (degrees)	Resulting deadband width (degrees)	Resulting limit cycle period (sec)
0	±0.5	0.053	413
0	±1.0	0.027	199
0	±1.5	0.017	131
0	±2.0	0.013	98
0	±2.5	0.011	78
0	±3.0	0.008	64
0	±3.5	0.007	55
0	±4.0	0.006	48
0	±4.5	0.006	43
0	±5.0	0.003	33

*S-IVB attitude control system with minimum pulse duration of 50ms and 150-pound-thrust jets used.

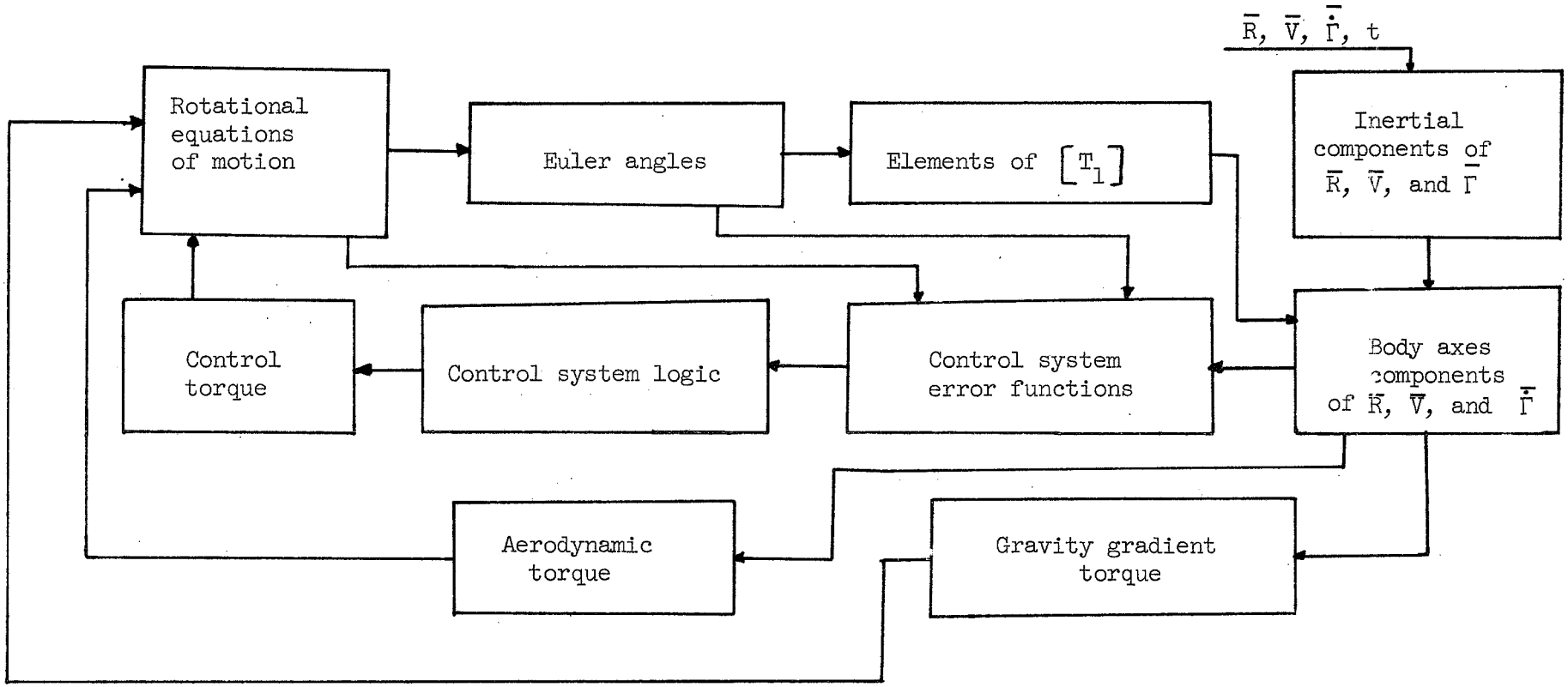

Figure 1.- Block diagram of mathematical model.

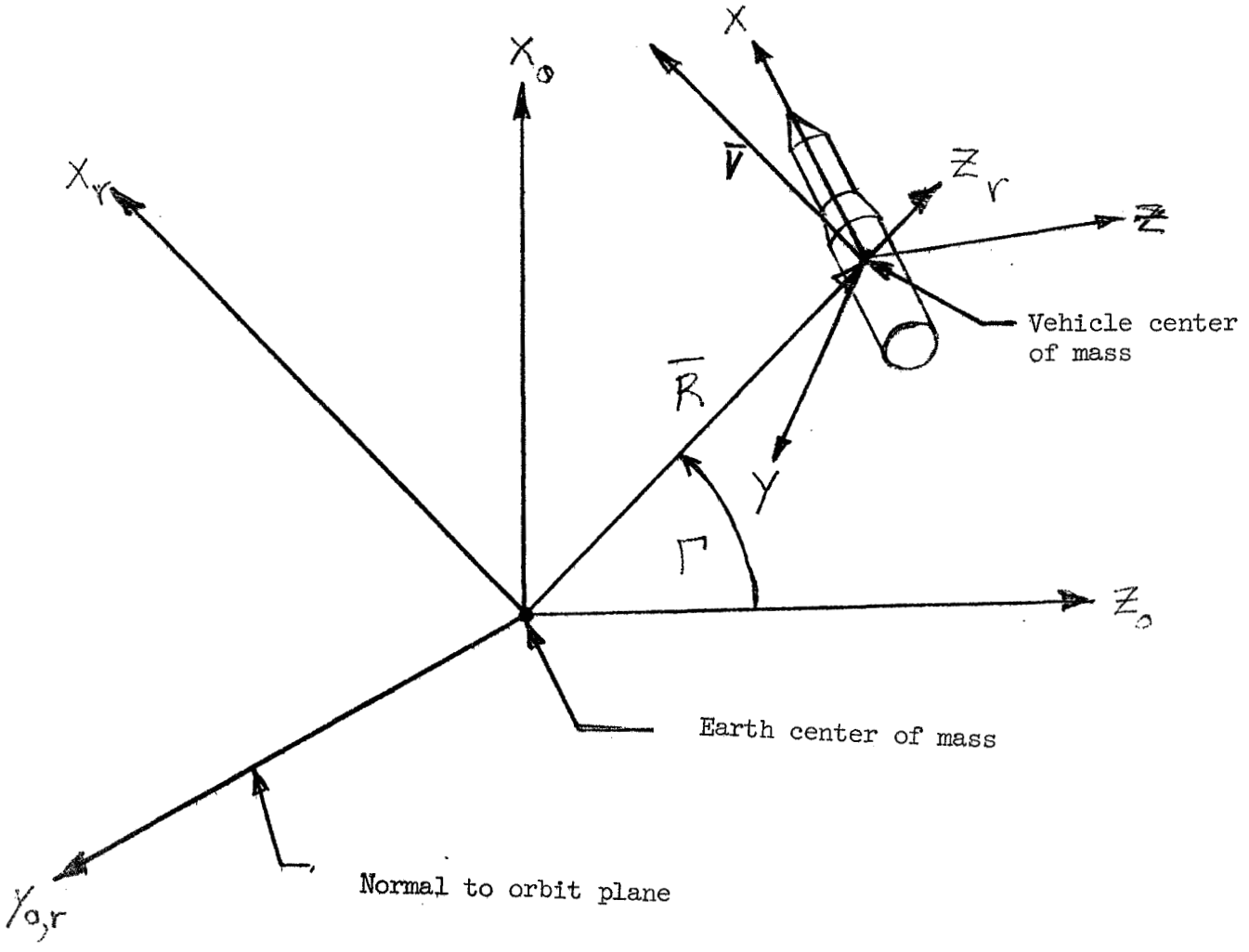

Figure 2.- Coordinate systems utilized to analyze angular motions of Apollo/S-IVB in earth orbit.

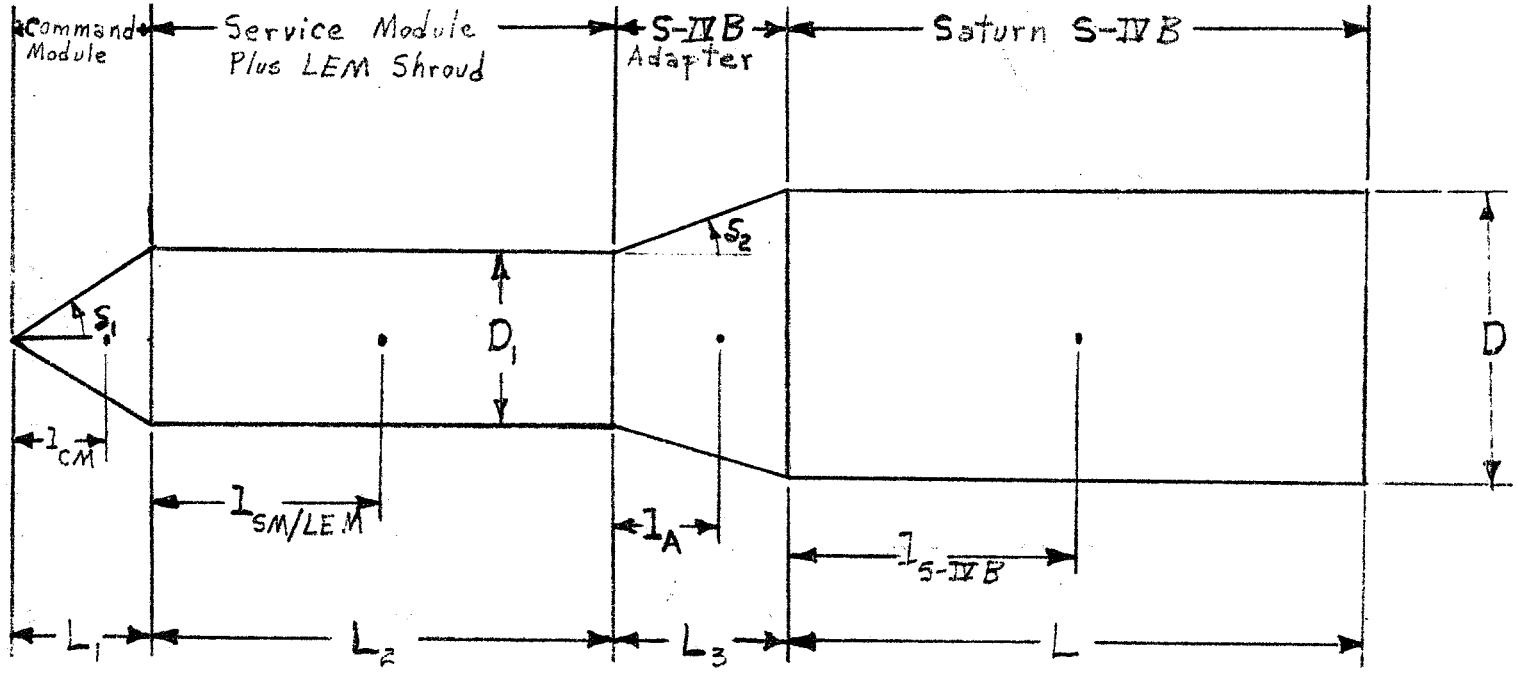

Figure 3.- Configuration used to represent Apollo/S-IVB for aerodynamic computations.

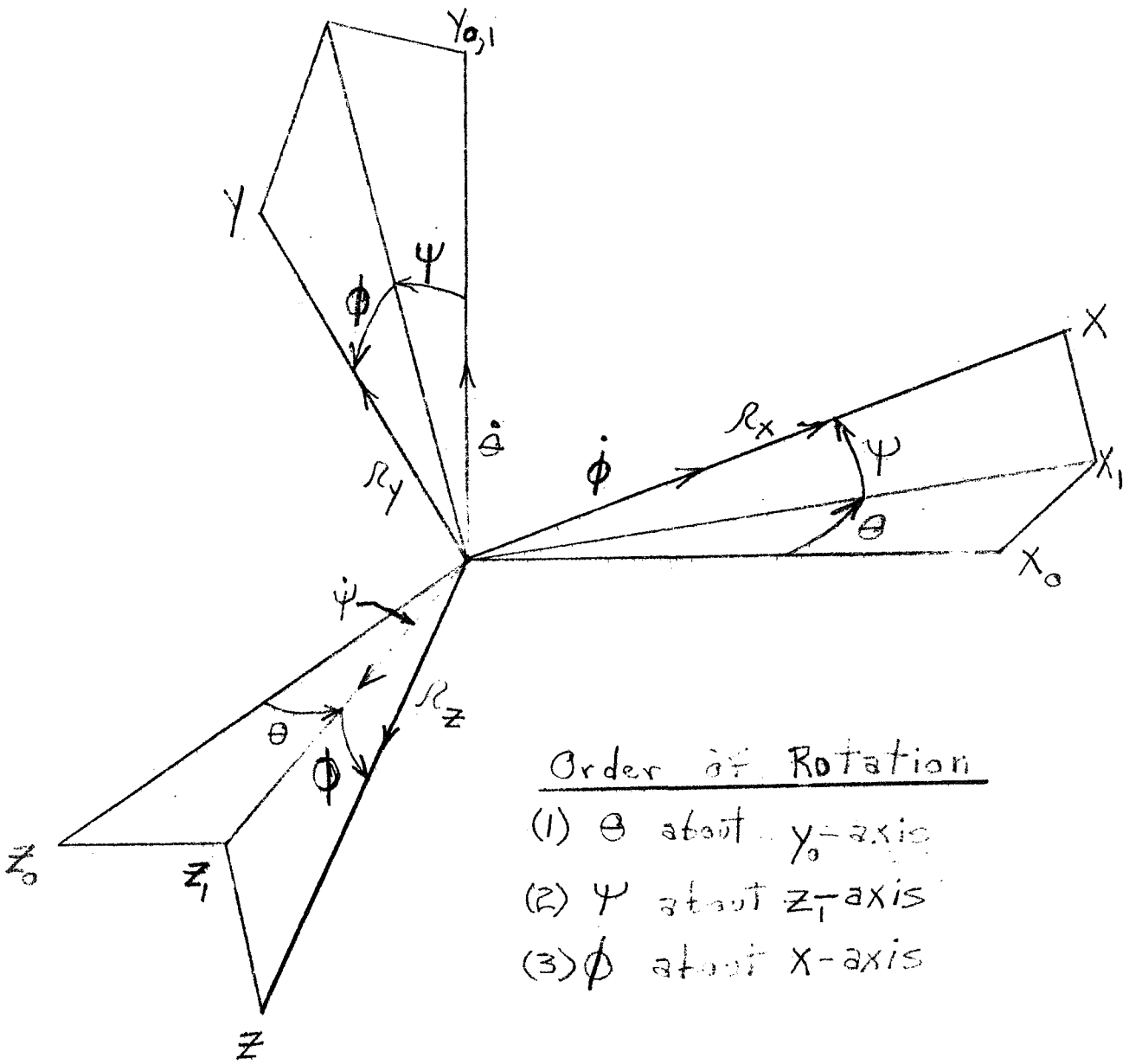

Figure 4.- Euler angles defining attitude of vehicle relative to inertial space.

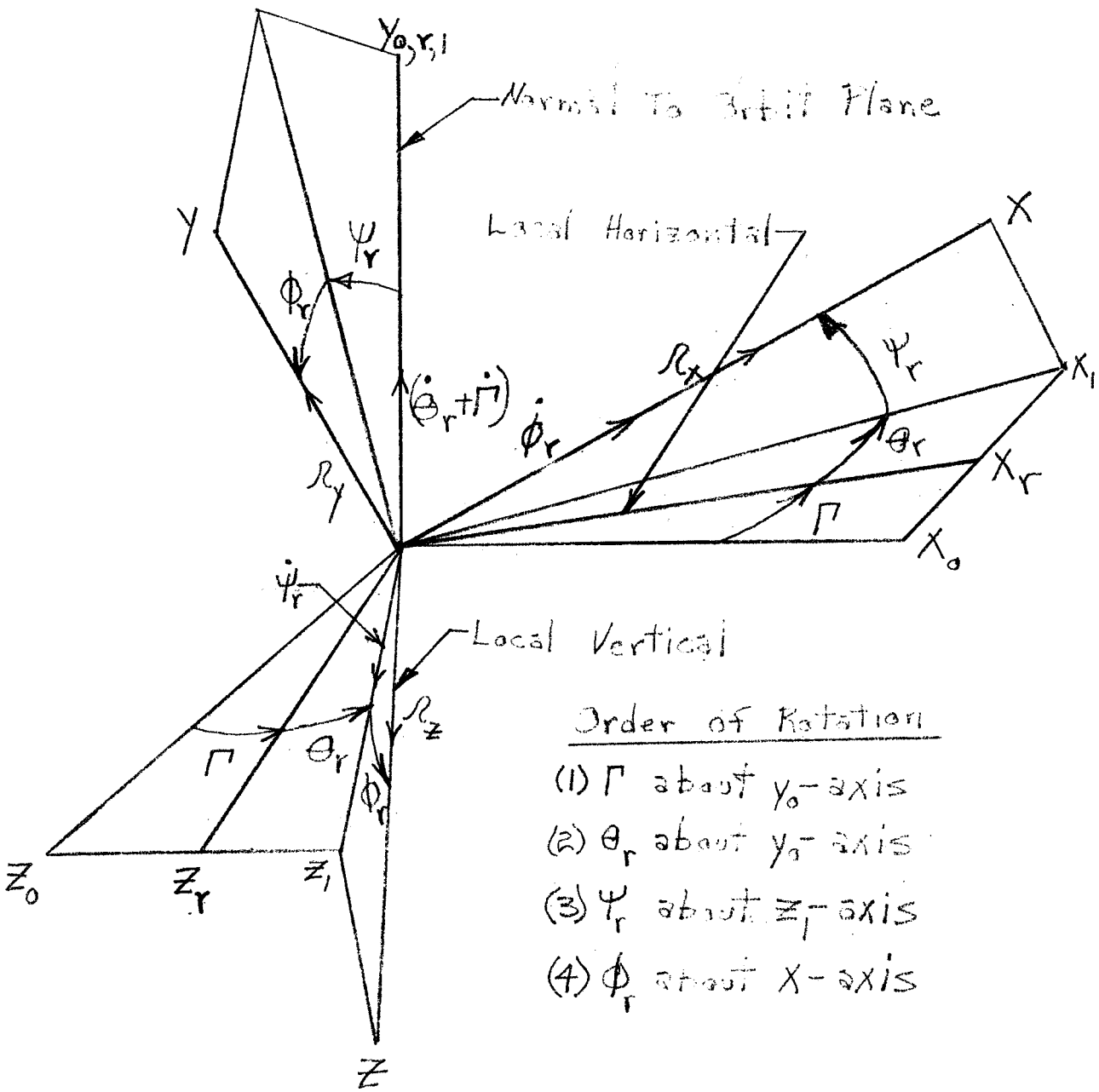

Figure 5.- Euler angles defining attitude of vehicle relative to local vertical.

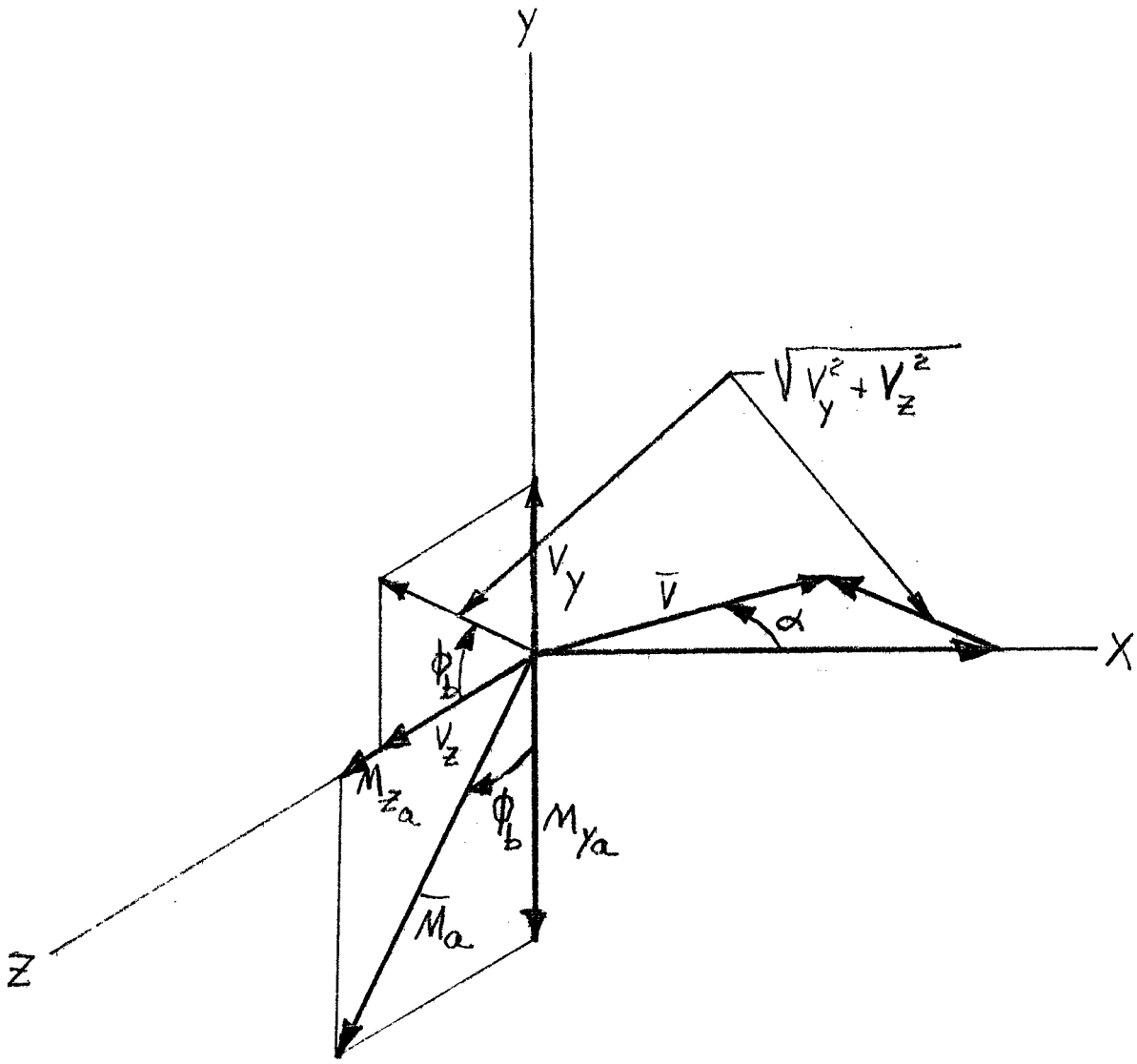

Figure 6.- Orientation of resultant velocity and aerodynamic torque vectors relative to vehicle body axes.

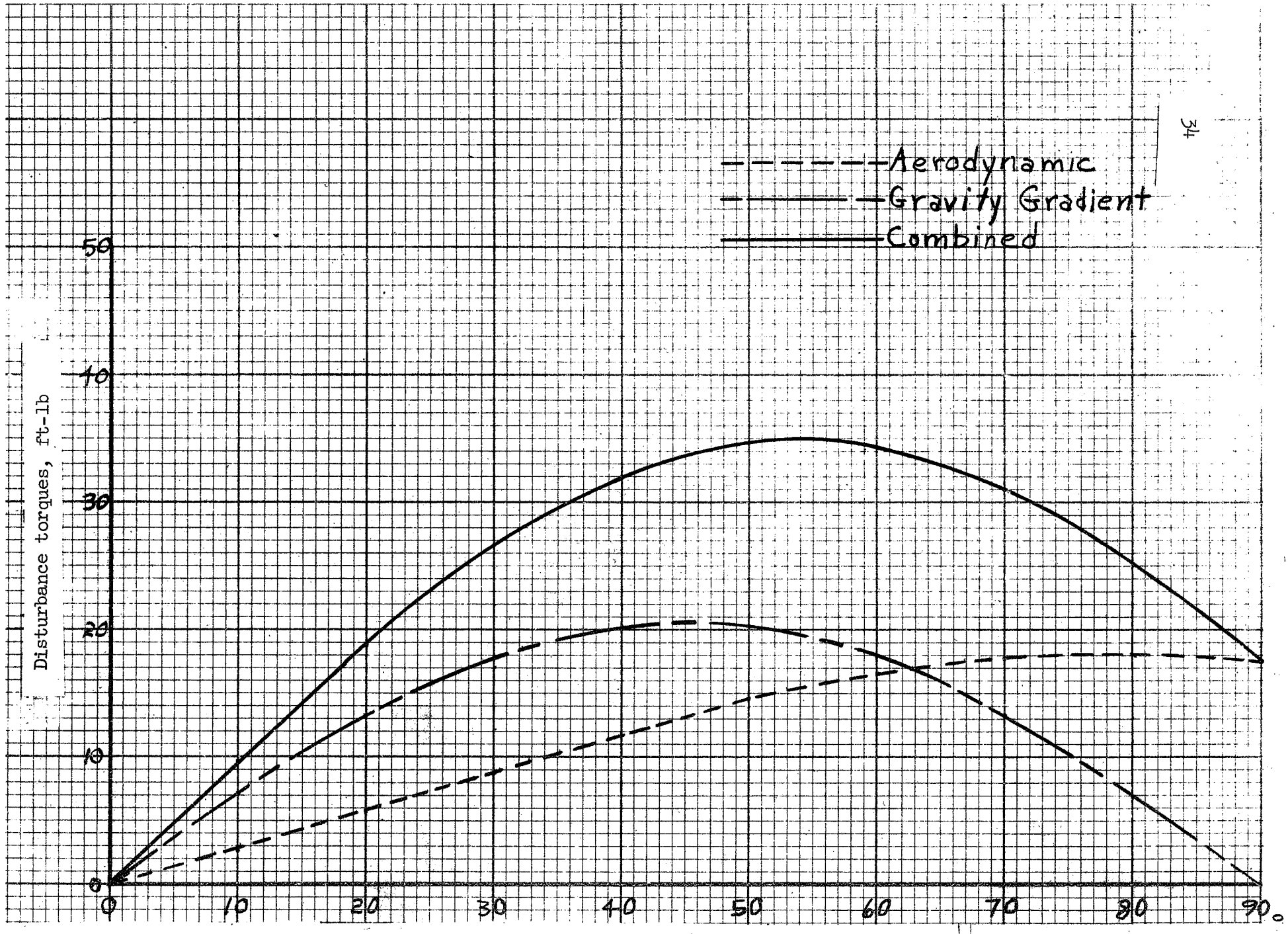

Figure 7.- Disturbance torques acting on Apollo/S-IVB in a 100-nautical-mile circular orbit about the earth.

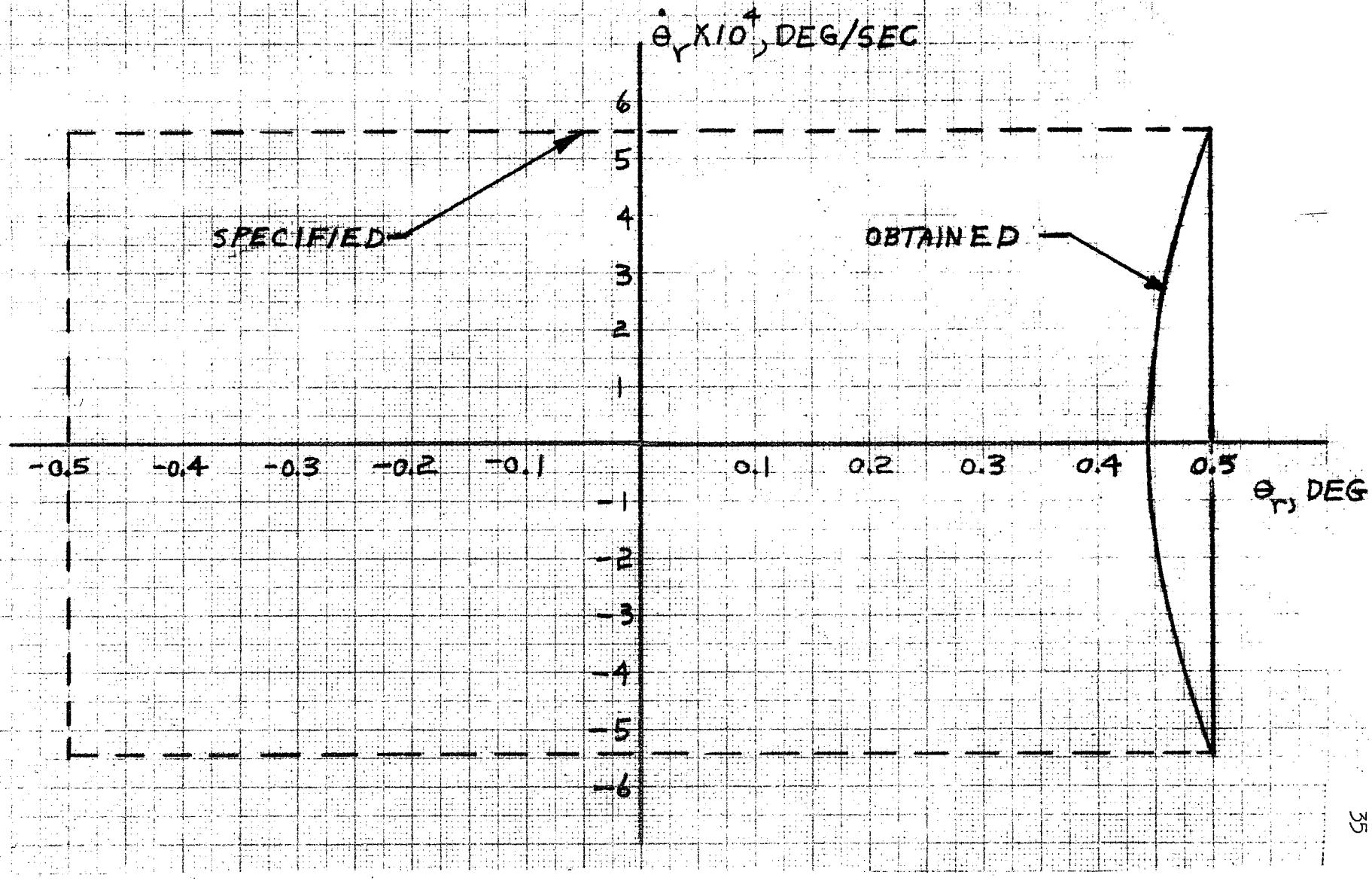

Figure 8.- Comparison of desired and achieved pitch-axis phase plane trajectory of Apollo/S-IVB in a 100-nautical-mile circular orbit about the earth.

APPENDIX A

THEORETICAL STATIC AERODYNAMIC FORCE COEFFICIENTS AND CENTERS OF PRESSURE FOR CERTAIN SYMMETRICAL BODIES OF REVOLUTION IN FREE-MOLECULE FLOW

RIGHT CIRCULAR CONE

Force Coefficients

Consider a body having a perfectly smooth surface to be moving in a highly rarefied gas, that is, a gas in which the frequency of collisions between individual molecules is negligibly small. According to reference 5, if a sufficient number of molecules are present to determine the macroscopic properties of the gas (pressure, temperature, density, et cetera), the condition is described as free-molecule flow. Near the surface of the body the two streams of incident and emergent molecules experience little interaction. In this case, the air molecules are said to reflect specularly; that is, the molecules are assumed to be smooth, perfectly elastic spheres which will rebound from a smooth surface at the same angle at which they strike. The behavior is illustrated in figure A-1 for a stream of air molecules impinging on a surface element of a right circular cone.

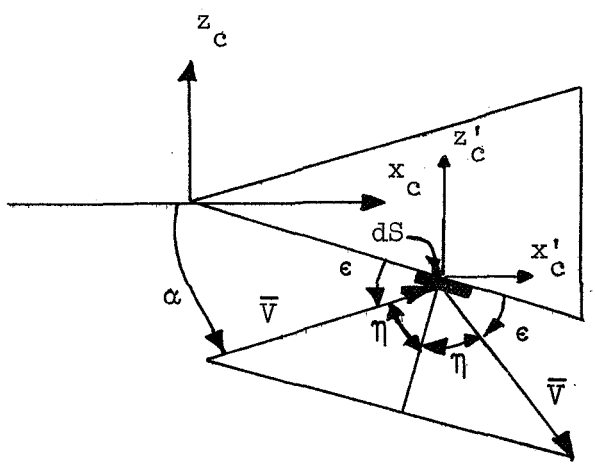

Figure A-1

In order to deflect the stream of incident molecules through the angle 2ε shown in figure A-1, the surface element ds must impart a velocity component

$$V_p = 2\left|\overline{V}\right| \cos \eta = 2V \cos \eta \tag{A1}$$

to the stream perpendicular to the surface element. If the velocity change is assumed to occur in unit time, the force exerted on the surface element due to the momentum change of the stream of molecules

$$dF = MV_p \tag{A2}$$

where

$$M = \rho V_p ds \tag{A3}$$

Substituting equations (A1) and (A3) into equation (A2),

$$dF = 4\rho V^2 \cos^2 \eta ds \tag{A4}$$

But ρ and V can be expressed in terms of dynamic pressure

$$q = \frac{1}{2} \rho V^2 \tag{A5}$$

Substituting equation (A5) into equation (A4),

$$dF = 8q \cos^2 \eta ds \tag{A6}$$

For a right circular cone, the position of a surface element is shown in figure A-2.

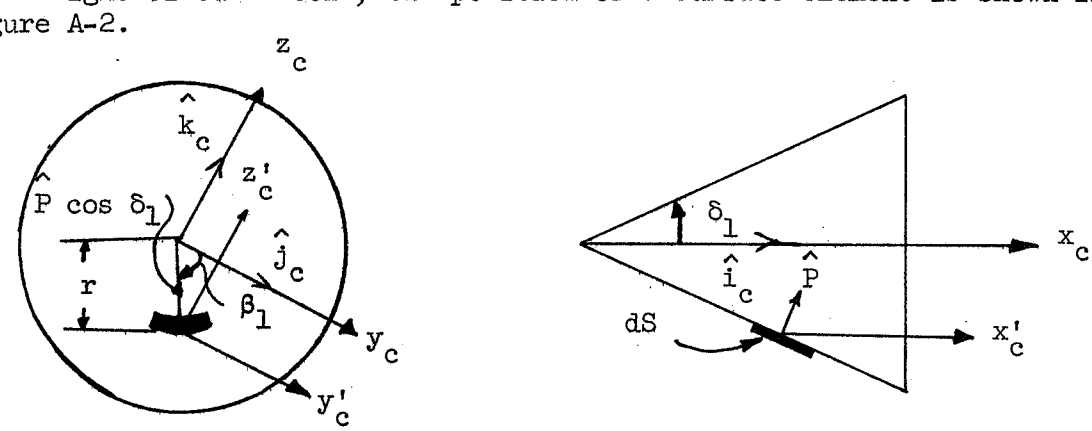

Figure A-2

In order to determine the aerodynamic force acting on the element, the angle η can be expressed as follows. From figure A-2, a unit vector perpendicular to the element of surface area

$$\hat{P} = P_{x_c'}\,\hat{i}_c + P_{y_c'}\,\hat{j}_c + P_{z_c'}\,\hat{k}_c \tag{A7}$$

and the velocity vector

$$\overline{V} = V_{x_c'}\,\hat{i}_c + V_{y_c'}\,\hat{j}_c + V_{z_c'}\,\hat{k}_c \tag{A8}$$

The components of $\overline{P}$ along the body axes are

$$\left.\begin{aligned} P_{x_c'} &= P \sin \delta_1 \\ P_{y_c'} &= -P \cos \delta_1 \operatorname{cox} \beta_1 \\ P_{z_c'} &= -P \operatorname{cox} \delta_1 \sin \beta_1 \end{aligned}\right\} \tag{A9}$$

and the components of $\overline{V}$ along the same axes are

$$\left.\begin{aligned} V_{x_c'} &= V \cos \alpha \\ V_{y_c'} &= 0 \\ V_{z_c'} &= V \sin \alpha \end{aligned}\right\} \tag{A10}$$

Since η is the angle between $\hat{P}$ and $\overline{V}$, it can be obtained from the dot product

$$\overline{V} \cdot \hat{P} = VP \cos \eta = V_{x_c'}\,P_{x_c'} + V_{y_c'}\,P_{y_c'} + V_{z_c'}\,P_{z_c'} \tag{A11}$$

Substituting equations (A9) and (A10) into equation (A11),

$$VP \cos \eta = VP \cos \alpha \sin \delta_1 - VP \cos \delta_1 \sin \beta_1 \sin \alpha$$

or

$$\cos \eta = \cos \alpha \sin \delta_1 - \cos \delta_1 \sin \beta_1 \sin \alpha \tag{A12}$$

Substituting equation (A12) into equation (A6), the resultant force acting on the surface element is

$$dF = 8q \left(\cos \alpha \sin \delta_1 - \cos \delta_1 \sin \beta_1 \sin \alpha\right)^2 ds \tag{A13}$$

The resultant force can be divided into a normal force dN along the z_c-axis and an axial force dC along the x_c-axis,

$$dN = -dF \cos \delta_1 \sin \beta_1 \tag{A14}$$

$$dC = dF \sin \delta_1 \tag{A15}$$

If the body possesses homogeneous mass distribution, the center of mass is located on the axis of symmetry, or the x_c-axis of figure A-1. Since only the moment produced by the resultant aerodynamic force is of interest in the present analysis and since the axial force acts through the center of mass, the axial force equation, equation (A15), will not be developed further.

The element of area shown in figure A-1 can be seen to be

$$dS = \frac{r d\beta_1 dx_c}{\cos \delta_1} \tag{A16}$$

Substituting equation (A16) into equation (A14),

$$dN = dFr \sin \beta d\beta_1 dx_c / dS \tag{A17}$$

When $\alpha \leq \delta_1$, the entire surface of the cone is exposed to the flow. However, when $\alpha > \delta_1$, a portion of the surface is shielded from the flow. According to impact theory, the pressure in the shielded region is zero and thus contributes nothing to the aerodynamic force. The boundary line separating the exposed region from the shielded region is the locus of points along the surface at which the velocity is tangent to the surface. Thus, at these points, the velocity vector $\overline{V}$ is perpendicular to the area $\hat{P}$ and $\cos \eta_u = 0$.

To determine β_1 at points along the boundary, equation (A12) can be written

$$\cos \eta_u = \cos \alpha \sin \delta_1 - \sin \alpha \cos \delta_1 \sin \beta_{1_u} = 0 \tag{A18}$$

or rearranging and solving equation (A18) for β_{1_u}

$$\beta_{1_u} = \sin^{-1} \frac{\tan \delta_1}{\tan \alpha} \tag{A19}$$

The resultant normal force acting on the body can be found by integrating equation (A17) over the exposed surface area, that is,

$$N = -\int_0^{x_u} \int_{-\frac{\pi}{2}}^{\beta_{1_u}} dFr \sin \beta_1 d\beta_1 dx_c \Big/ dS \tag{A20}$$

Substituting equation (A13) into equation (A20),

$$N = -8q \int_0^{x_{c_u}} \int_{-\frac{\pi}{2}}^{\beta_{1_u}} (\cos \alpha \sin \delta_1 - \sin \alpha \cos \delta_1 \sin \beta_1)^2 \sin \beta_1 d\beta_1 dx_c \tag{A21}$$

In order to integrate equation (A21), it is convenient to define a normal force coefficient per unit length of the body.

$$C'_{N_C} = \frac{dC_{N_C}}{d(x_c/D_1)} \tag{A22}$$

where

$$C_{N_C} = \frac{N}{qS} = \frac{N}{q\pi r_1^{\,2}} \tag{A23}$$

or, differentiating equation (A23),

$$dC_{N_C} = \frac{dN}{q\pi r_1^{\,2}} \tag{A24}$$

Substituting equation (A24) into equation (A22),

$$C'_{N_C} = \frac{1}{q\pi r_1^{\,2}} \frac{dN}{d(x_c/D_1)} \tag{A25}$$

Differentiating equation (A21) with respect to x,

$$\frac{dN}{dx} = -\,8qr \int_{-\frac{\pi}{2}}^{\beta_{1_u}} (\cos\alpha \sin\delta_1 - \sin\alpha \cos\delta_1 \sin\beta_1)^2 \sin\beta_1 d\beta_1 \tag{A26}$$

since r is a function of x_c only.

But

$$\frac{dN}{dx} = \frac{1}{D_1} \frac{dN}{d(x_c/D_1)} \tag{A27}$$

Thus, the right side of equation (A26) can be multiplied by D_1 and the resulting quantity substituted into equation (A25), yielding

$$C'_{N_C} = \frac{-8qrD_1}{q\pi r_1^{\,2}} \int_{-\frac{\pi}{2}}^{\beta_{1_u}} (\cos\alpha \sin\delta_1 - \sin\alpha \cos\delta_1 \sin\beta_1)^2 \sin\beta_1 d\beta_1 \tag{A28}$$

Substituting $D_B = 2r_B$ and expanding equation (A28),

$$C'_{N_C} = \frac{-16}{\pi} \frac{r}{r_1} \int_{-\frac{\pi}{2}}^{\beta_{1_u}} (\cos^2\alpha \sin^2\delta_1 - 2 \sin\alpha \cos\alpha \sin\delta_1 \cos\delta_1 \sin\beta_1$$

$$+ \sin^2\alpha \cos^2\delta_1 \sin^2\beta_1) \sin\beta_1 d\beta_1 \tag{A29}$$

Since the cone angle δ_1 is constant, straightforward integration of equation (A29) holding α constant during the integration yields

$$C'_{N_C} = \frac{8}{\pi}\frac{r}{r_1}\left\{\frac{1}{2}\left(\beta_u + \frac{\pi}{2}\right)\sin 2\alpha \sin 2\delta_1 + \cos \beta_{1_u}\left[2\cos^2\alpha \sin^2 \delta_1 - \frac{1}{2}\sin 2\alpha \sin 2\delta_1 \sin \beta_{1_u} + \frac{2}{3}\sin^2\alpha \cos^2 \delta_1 \left(\sin^2 \beta_{1_u} + 2\right)\right]\right\} \tag{A30}$$

For the case in which $\alpha \leq \delta_1$, the entire surface of the cone is exposed to the flow. In this case the upper limit of integration is $\beta_{1_u} = \frac{\pi}{2}$ and equation (A30) reduces to

$$C'_{N_C} = \frac{4r}{r_1}\sin 2\alpha \sin 2\delta_1 \tag{A31}$$

When $\alpha > \delta_1$, equation (A19) must be utilized to evaluate equation (A30). It can be seen from equation (A19) that

$$\cos \beta_{1_u} = \frac{\sqrt{\tan^2\alpha - \tan^2 \delta_1}}{\tan \alpha} \tag{A32}$$

Substituting equation (A32) into equation (A30) and rearranging,

$$C'_{N_C} = \frac{8}{\pi}\frac{r}{r_1}\cos^2 \delta_1 \sin 2\alpha \left\{\left(\beta_{1_u} + \frac{\pi}{2}\right)\tan \delta_1 + \frac{1}{3}\cos \beta_{1_u}\left[\cot \alpha \tan^2 \delta_1 + 2\tan \alpha\right]\right\} \tag{A33}$$

It should be remembered that equations (A31) and (A33) were derived on the assumption that centrifugal forces resulting from flow over a curved surface are negligible and that expansion flow regions contribute nothing to the aerodynamic force.

The total normal force coefficient can be obtained from equation (A22),

$$C_{N_C} = \int_0^{\frac{L_1}{D_1}} C'_{N_C} \, d\left(\frac{x_c}{D_1}\right) \tag{A34}$$

When $\alpha \leq \delta_1$, substitution of equation (A31) into equation (A34) yields

$$C_{N_C} = 4 \sin 2\alpha \sin 2\delta_1 \int_0^{\frac{L_1}{D_1}} \frac{r}{r_1} \, d\left(\frac{x_c}{D_1}\right) \tag{A35}$$

But, as shown in figure A-3,

$$\frac{r}{r_1} = \frac{x_c}{L_1} \tag{A36}$$

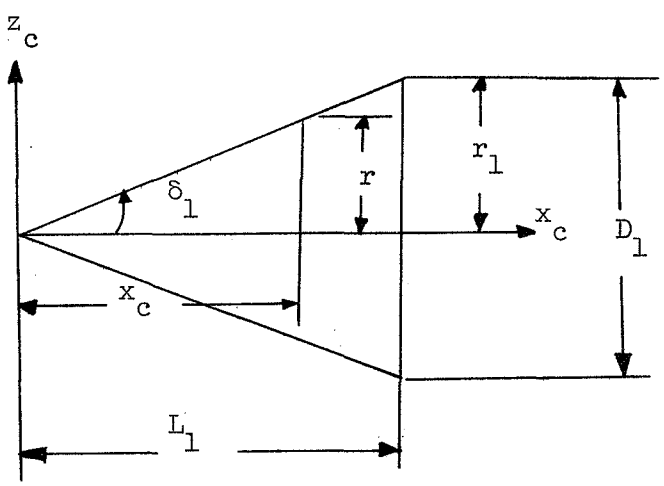

Figure A-3

Multiplying and dividing equation (A36) by D_1,

$$\frac{r}{r_1} = \frac{D_1}{L_1}\left(\frac{x_c}{D_1}\right) \tag{A37}$$

Also from figure A-3,

$$\frac{D_1}{L_1} = 2 \tan \delta_1 \tag{A38}$$

Thus

$$\frac{r}{r_1} = 2 \frac{x_c}{D_1} \tan \delta_1 \tag{A39}$$

Substituting equation (A39) into equation (A35), replacing $\sin 2\delta_1$ by $2 \sin \delta_1 \cos \delta_1$,

$$C_{N_C} = 16 \sin^2 \delta_1 \sin 2\alpha \int_0^{\frac{L_1}{D_1}} \left(\frac{x_c}{D_1}\right) d\left(\frac{x_c}{D_1}\right) \tag{A40}$$

Integrating equation (A40) and evaluating at the upper and lower limits,

$$C_{N_C} = 8 \left(\frac{L_1}{D_1}\right)^2 \sin^2 \delta_1 \sin 2\alpha \tag{A41}$$

But, from equation (A38),

$$\frac{L_1}{D_1} = \frac{1}{2} \frac{\cos \delta_1}{\sin \delta_1} \tag{A42}$$

Substituting equation (A42) into equation (A41),

$$C_{N_C} = 2 \cos^2 \delta_1 \sin 2\alpha \qquad \text{when} \quad \alpha \leq \delta_1 \tag{A43}$$

When $\alpha > \delta_1$, substitution of equation (A39) into equation (A30) followed by substitution of the resulting expression into equation (A34) yields, after integration along x_c,

$$C_{N_C} = \frac{2}{\pi} \cot \delta_1 \left\{ \frac{1}{2}\left(\beta_{1_u} + \frac{\pi}{2}\right) \sin 2\alpha \sin 2\delta_1 + \cos \beta_{1_u} \left[2 \cos^2 \alpha \sin^2 \delta_1 \right.\right.$$

$$\left.\left. - \frac{1}{2} \sin 2\alpha \sin 2\delta_1 \sin \beta_{1_u} + \frac{2}{3} \sin^2 \alpha \cos^2 \delta_1 \left(\sin^2 \beta_{1_u} + 2\right)\right]\right\}$$

$$\text{when} \quad \alpha > \delta_1 \tag{A44}$$

It should be remembered that C_{N_C} as evaluated from equation (A43) or (A44) is based on the maximum cross-sectional area of the cone, $\pi D_1^2/4$.

Center of Pressure

In order to determine the aerodynamic moment on a right circular cone from the normal force coefficient, it is necessary to know the location of the center of pressure. This can be determined from the expression

$$l_C = \frac{\text{moment}}{\text{normal force}} = \frac{M}{N} \tag{A45}$$

The normal force on a unit length of the cone is, from equation (A25)

$$dN = C'_{N_C} \, d\left(\frac{x_c}{D_1}\right) q\pi r_1^2 \tag{A46}$$

and the resulting moment about the cone vertex

$$dM = x_c C'_{N_C} \, d\left(\frac{x_c}{D_1}\right) q\pi r_1^2 \tag{A47}$$

Integrating equation (A47) over the length of the cone,

$$M = D_1 \, q\pi r_1^2 \int_0^{\frac{L_1}{D_1}} \left(\frac{x_c}{D_1}\right) C'_{N_C} \, d\left(\frac{x_c}{D_1}\right) \tag{A48}$$

Substituting equations (A31) and (A39) into equation (A48),

$$M = 16\ D_1\ q\pi r_1^{\ 2}\ \sin 2\alpha\ \sin^2\delta_1 \int_0^{\frac{L_1}{D_1}} \left(\frac{x_c}{D_1}\right)^2 d\left(\frac{x_c}{D_1}\right) \tag{A49}$$

Integrating equation (A49),

$$M = \frac{16}{3}\ D_1\ q\pi r_1^{\ 2}\ \sin 2\alpha\ \sin^2\ \delta_1 \left(\frac{L_1}{D_1}\right)^3 \tag{A50}$$

The resultant normal force on the cone

$$N = C_{N_C}\ q\pi r_1^{\ 2} \tag{A51}$$

Substituting equations (A41), (A50), and (A51) into equation (A45) and simplifying,

$$l_C = \frac{2}{3}\ L_1 \tag{A52}$$

where l_C is measured from the cone vertex.

RIGHT CIRCULAR CONE FRUSTUM

Normal Force Coefficient

The normal force coefficient for a right circular cone frustum can be obtained from the expressions for the normal force coefficients of a right circular cone developed above. This is accomplished by subtracting the coefficient of the small cone shown in figure A-4 from the coefficient of the large cone. When $\alpha \leq \delta_2$, the coefficient of the small cone is seen from equation (A43) and figure A-4 to be

$$C_{N_S} = 2\ \cos^2\ \delta_2\ \sin 2\alpha \tag{A53}$$

where C_{N_S} is based on the area $\pi D_1^{\ 2}/4$.

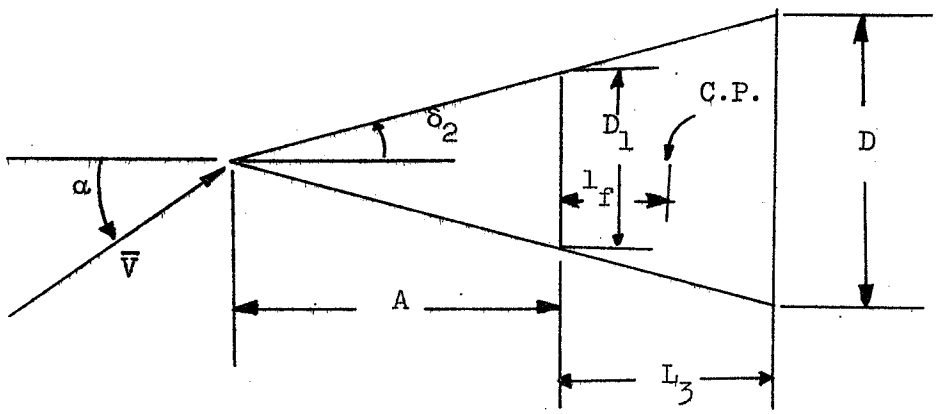

Figure A-4

Similarly, the coefficient for the large cone

$$C_{N_L} = 2 \cos^2 \delta_2 \sin 2\alpha \tag{A54}$$

where C_{N_L} is based on the area $\pi D^2/4$.

Before subtracting C_{N_S} from C_{N_L} to determine the coefficient of the frustum, both must be based on the same area. If the area $\pi D^2/4$ is chosen, C_{N_S} must be multiplied by the ratio $(\pi D_1^2/4)/(\pi D^2/4) = D_1^2/D^2$,

$$C_{N_S} = 2 \left(\frac{D_1}{D}\right)^2 \cos^2 \delta_2 \sin 2\alpha \tag{A55}$$

Then the frustum coefficient

$$C_{N_f} = C_{N_L} - C_{N_S} \tag{A56}$$

Substituting equations (A54) and (A55) into equation (A56),

$$C_{N_f} = 2\left[1 - \left(\frac{D_1}{D}\right)^2\right]\cos^2\delta_2 \sin 2\alpha \qquad \alpha \leq \delta_2 \tag{A57}$$

When $\alpha > \delta_2$, the above procedure can be applied to equation (A44), replacing δ_1 and β_{1_u} by δ_2 and β_{2_u} respectively in equation (A44) to obtain,

$$\begin{aligned} C_{N_f} = \frac{2}{\pi}\cot\delta_2\left[1 - \left(\frac{D_1}{D}\right)^2\right]\Bigg\{&\frac{1}{2}\left(\beta_{2_u} + \frac{\pi}{2}\right)\sin 2\alpha \sin 2\delta_2 \\ &+ \cos\beta_{2_u}\Bigg[2\cos^2\alpha \sin^2\delta_2 - \frac{1}{2}\sin 2\alpha \sin 2\delta_2 \sin\beta_{2_u} \\ &+ \frac{2}{3}\sin^2\alpha \cos^2\delta_2 \left(\sin^2\beta_{2_u} + 2\right)\Bigg]\Bigg\} \qquad \alpha > \delta_2 \end{aligned} \tag{A58}$$

where β_{2_u} is obtained from equation (A32) by replacing δ_1 and β_{1_u} by δ_2 and β_{2_u} respectively. It should be remembered that C_{N_f} as determined from equation (A57) or (A58) is based on the area $\pi D^2/4$.

Center of Pressure

The center of pressure of the frustum can be determined using equation (A52) with the appropriate subscripts for the small and large cones of figure 4. The center of pressure of the large cone

$$l_L = \frac{2}{3}(A + L_3) \tag{A59}$$

and the center of pressure of the small cone

$$l_S = \frac{2}{3}A \tag{A60}$$

The center of pressure distance from the cone vertex is determined by the ratio of large-cone moment minus small-cone moment to large-cone normal force minus small-cone normal force. Symbolically,

$$A + l_f = \frac{M_L - M_S}{N_L - N_S} \tag{A61}$$

But

$$\left.\begin{aligned} N_L &= C_{N_L}\, q\, \frac{\pi D^2}{4} \\ N_S &= C_{N_S}\, q\, \frac{\pi D_1^{\,2}}{4} \end{aligned}\right\} \tag{A62}$$

and

$$\left.\begin{aligned} M_L &= N_L\, l_L = C_{N_L}\, q\, \frac{\pi D^2}{4}\, l_L \\ M_S &= N_S\, l_S = C_{N_S}\, q\, \frac{\pi D_1^{\,2}}{4}\, l_S \end{aligned}\right\} \tag{A63}$$

Substituting equations (A62) and (A63) into equation (A61) and simplifying,

$$A + l_f = \frac{C_{N_L}\, D^2\, l_L - C_{N_S}\, D_1^{\,2}\, l_S}{C_{N_L}\, D^2 - C_{N_S}\, D_1^{\,2}} \tag{A64}$$

Substituting equations (A59) and (A60) into equation (A64) and simplifying,

$$A + l_f = \frac{2}{3}\, \frac{C_{N_L}\, D^2\, (A + L_3) - C_{N_S}\, D_1^{\,2}\, A}{C_{N_L}\, D^2 - C_{N_S}\, D_1^{\,2}} \tag{A65}$$

From equation (A43), replacing δ_1 by δ_2,

$$\left.\begin{aligned} C_{N_L} &= 2 \cos^2 \delta_2 \sin 2\alpha \\ C_{N_S} &= 2 \cos^2 \delta_2 \sin 2\alpha \end{aligned}\right\} \tag{A66}$$

Substituting equation (A66) into equation (A65) and simplifying

$$l_f = \frac{2}{3} \frac{D^2 (A + L_3) - D_1^{\,2} A}{(D^2 - D_1^{\,2})} - A \tag{A67}$$

From figure A-4, using a property of similar triangles,

$$\frac{A}{D_1} = \frac{A + L_3}{D} \tag{A68}$$

or, solving for A,

$$A = \frac{L_3 D_1}{D - D_1} \tag{A69}$$

Substituting equation (A69) into equation (A67) and rearranging,

$$l_f = \frac{L_3 (D_1 + 2D)}{3 (D_1 + D)} \tag{A70}$$

RIGHT CIRCULAR CYLINDER

Normal Force Coefficient

The normal force coefficient per unit length of a right circular cylinder can be obtained from equations (A19) and (A30) developed above for a right circular cone. The procedure is simply to equate the cone

angle δ_1 in equations (A19) and (A30) to zero and determine the resulting expressions. From equation (A19), with $\delta_1 = 0$,

$$\beta_{3_u} = 0 \tag{A71}$$

Substituting equation (A71) into equation (A30), with $\delta_1 = 0$ and $r = r_1 = r_{cyl}$ for the cylinder,

$$C'_{N_{cyl}} = \frac{32}{3\pi} \sin^2 \alpha \tag{A72}$$

Using the nomenclature shown in figure A-5,

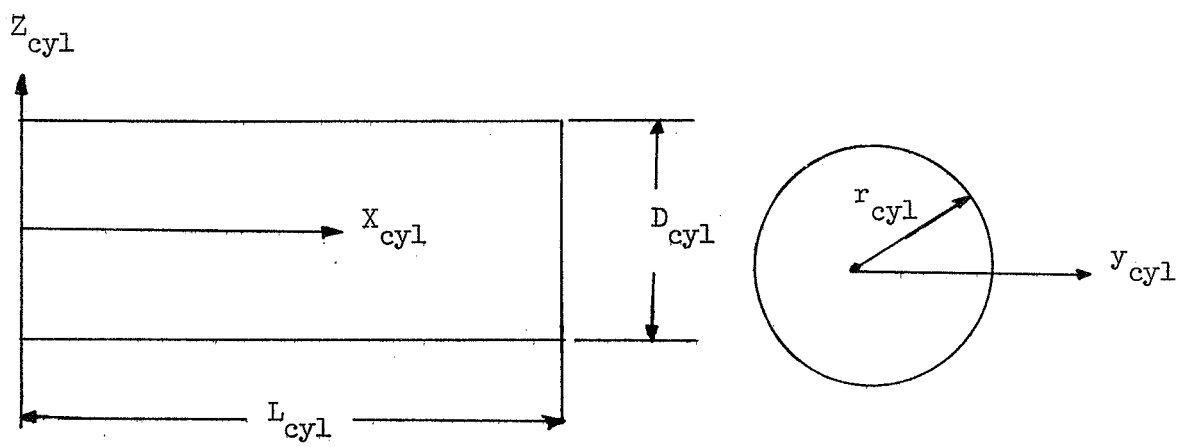

Figure A-5

the normal force coefficient for the complete cylinder

$$C_{N_{cyl}} = \int_0^{\frac{L_{cyl}}{D_{cyl}}} C'_{N_{cyl}} \, d\left(\frac{X_{cyl}}{D_{cyl}}\right) \tag{A73}$$

Substituting equation (A72) into equation (A73) and integrating,

$$C_{N_{cyl}} = \frac{32}{3\pi} \frac{L_{cyl}}{D_{cyl}} \sin^2 \alpha \tag{A74}$$

where $C_{N_{cyl}}$ is based on the area $\pi D^2_{cyl}/4$.

Center of Pressure

The elemental torque due to the normal force acting on a unit length of the cylinder

$$dM_{cyl} = X_{cyl}\, C'_{N_C}\, d\left(\frac{X_{cyl}}{D_{cyl}}\right) q\pi r^2_{cyl} \tag{A75}$$

and the resultant torque

$$M_{cyl} = D_{cyl} \int_0^{\left(\frac{L_{cyl}}{D_{cyl}}\right)} C'_{N_C}\left(\frac{X_{cyl}}{D_{cyl}}\right) d\left(\frac{X_{cyl}}{D_{cyl}}\right) q\pi r^2_{cyl} \tag{A76}$$

Substituting equation (A72) into equation (A76) and performing the indicated integration,

$$M_{cyl} = \frac{16}{3\pi}\,\frac{L^2_{cyl}}{D_{cyl}}\, q\pi r^2_{cyl}\, \sin^2\alpha \tag{A77}$$

The resultant normal force acting on the cylinder

$$N_{cyl} = C_{N_{cyl}}\, q\pi r^2_{cyl} \tag{A78}$$

Substituting equation (A74) into equation (A78)

$$N_{cyl} = \frac{32}{3\pi}\,\frac{L_{cyl}}{D_{cyl}}\, q\pi r^2_{cyl}\, \sin^2\alpha \tag{A79}$$

The center of pressure distance from the front of the cylinder

$$l_{cyl} = \frac{M_{cyl}}{N_{cyl}} \tag{A80}$$

Substituting equations (A77) and (A79) into equation (A80) and simplifying,

$$l_{cyl} = \frac{1}{2} L_{cyl} \tag{A81}$$

APPENDIX B

GRAVITY GRADIENT TORQUE ACTING ON A VEHICLE IN AN INVERSE SQUARE FORCE FIELD

The force due to gravity acting on an element of mass dm in the vehicle shown in figure B-1 can be written vectorially as:

$$d\bar{F}_G = -\frac{Kdm\bar{r}_m}{r_m^3} \tag{B1}$$

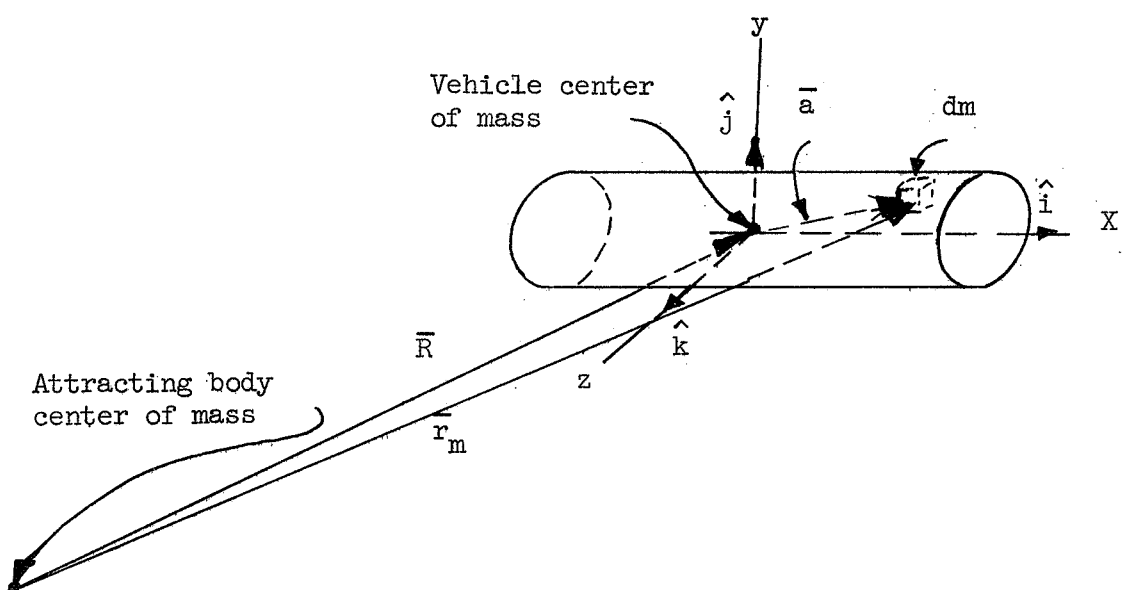

Figure B-1

But, by vector addition (see fig. B-1),

$$\bar{r}_m = \bar{R} + \bar{a} \tag{B2}$$

where

$$\bar{R} = R_x\,\hat{i} + R_y\,\hat{j} + R_z\,\hat{k} \tag{B3}$$

$$\bar{a} = x\hat{i} + y\hat{j} + z\hat{k} \tag{B4}$$

Substituting equations (B3) and (B4) into equation (B2),

$$\bar{r}_m = (R_x + x)\hat{i} + (R_y + y)\hat{j} + (R_z + z)\hat{k} \tag{B5}$$

The incremental torque on the vehicle is, from reference 6,

$$d\bar{M}_G = \bar{a} \times d\,\bar{F}_G \tag{B6}$$

Substituting equations (B1), (B4), and (B5) into equation (B6) and using matrix notation

$$d\bar{M}_G = \frac{-Kdm}{r_m^{\,3}} \begin{vmatrix} \hat{i} & \hat{j} & \hat{k} \\ (x) & (y) & (z) \\ (R_x + x) & (R_y + y) & (R_z + z) \end{vmatrix} \tag{B7}$$

Expanding equation (B7) and simplifying,

$$d\bar{M}_G = \frac{-Kdm}{r_m^{\,3}} \left[\hat{i}\left(yR_z - zR_y\right) + \hat{j}\left(zR_x - xR_z\right) + \hat{k}\left(xR_y - yR_x\right) \right] \tag{B8}$$

In order to integrate equation (B8) over the mass of the vehicle, it is necessary to express the quantity $1/r^3$ as a function of R and a. An approximate expression of this form can be obtained in the following manner.

The dot product

$$\bar{r}_m \cdot \bar{r}_m = r_m^{\,2} = (\bar{R} + \bar{a}) \cdot (\bar{R} + \bar{a})$$

$$= \bar{R} \cdot \bar{R} + \bar{a} \cdot \bar{a} + 2\bar{R} \cdot \bar{a} \tag{B9}$$

Substituting equations (B3) and (B4) into equation (B9) and expanding,

$$r_m^{\,2} = R^2 \left[1 + (a/R)^2 + (2/R^2)\,(xR_x + yR_y + zR_z) \right] \tag{B10}$$

Assume now that $(a/R)^2 \ll 1$ and can be ignored in equation (B10). Thus,

$$r_m^{\,2} \simeq R^2\left[1 + (2/R^2)\,(xR_x + yR_y + zR_z)\right] \tag{B11}$$

Raising equation (B11) to the -3/2 power,

$$\frac{1}{r_m^{\,3}} \simeq \frac{1}{R^3}\left[1 + (2/R^2)\,(xR_x + yR_y + zR_z)\right]^{-\frac{3}{2}} \tag{B12}$$

Expanding equation (B12) by the binomial theorem, retaining only the first term of the expansion,

$$\frac{1}{r_m^{\,3}} \simeq \frac{1}{R^3}\left[1 - \frac{3}{R^2}\,(xR_x + yR_y + zR_z)\right] \tag{B13}$$

Combining equations (B8) and (B13), the components of $d\bar{M}$ along the x, y, and z-axes, respectively, are:

$$dM_{x_G} = \frac{-Kdm}{R^3}\left[1 - \frac{3}{R^2}\,(xR_x + yR_y + zR_z)\right]\left[yR_z - zR_y\right] \tag{B14}$$

$$dM_{y_G} = \frac{-Kdm}{R^3}\left[1 - \frac{3}{R^2}\,(xR_x + yR_y + zR_z)\right]\left[zR_x - xR_z\right] \tag{B15}$$

$$dM_{z_G} = \frac{-Kdm}{R^3}\left[1 - \frac{3}{R^2}\,(xR_x + yR_y + zR_z)\right]\left[xR_y - yR_x\right] \tag{B16}$$

Expanding equation (B14),

$$dM_{x_G} = \frac{-Kdm}{R^3}\Big[yR_z - zR_y - \frac{3}{R^2}\,(xyR_xR_z - xzR_xR_y + y^2R_yR_z - yzR_y^{\,2} + yzR_z^{\,2} - z^2R_yR_z)\Big] \tag{B17}$$

The total torque about the x-axis due to gravity gradient for any orientation of the vehicle relative to the attracting body can be found by integrating equation (B17) over the mass of the vehicle with R_x, R_y, and R_z held constant during the integration. Integrating equation (B17) term by term,

$$M_{x_G} = \frac{-K}{R^3}\left\{R_z \int ydm - R_y \int zdm \frac{-3}{R^2}\left[R_x R_z \int xydm\right.\right.$$

$$-R_x R_y \int xzdm + R_y R_z \int y^2 dm - R_y^2 \int yzdm$$

$$\left.\left. + R_z^2 \int yzdm - R_y R_z \int z^2 dm\right]\right\} \tag{B18}$$

Since the origin of the xyz-axis system is located at the center of mass of the vehicle (fig. B-1), it must necessarily follow that:

$$\int xdm = \int ydm = \int zdm = 0 \tag{B19}$$

to be consistent with the definition of center of mass. Substituting equation (B19) into equation (B18), then adding and subtracting $(3K/R^5)\ R_y R_z \int x^2 dm$ to the resulting expression yields:

$$M_{x_G} = \frac{3K}{R^5}\left\{R_x R_z \int xydm - R_x R_y \int xzdm\right.$$

$$+ R_y R_z \int (x^2 + y^2)\ dm - R_y R_z \int (x^2 + z^2)\ dm$$

$$\left. + (R_z^2 - R_y^2) \int yzdm\right\} \tag{B20}$$

But

$$\left.\begin{aligned} \int xydm &\equiv I_{xy} \\ \int xzdm &\equiv I_{xz} \\ \int yzdm &\equiv I_{yz} \end{aligned}\right\} \tag{B21}$$

$$\left.\begin{aligned} \int (y^2 + z^2)\ dm &\equiv I_x \\ \int (x^2 + z^2)\ dm &\equiv I_y \\ \int (x^2 + y^2)\ dm &\equiv I_z \end{aligned}\right\} \tag{B22}$$

Substituting equations (B21) and (B22) into equation (B20),

$$M_{x_G} = \frac{3K}{R^5}\left[R_x R_z I_{xy} - R_x R_y I_{xz} + (R_z{}^2 - R_y{}^2)\ I_{yz} + R_y R_z (I_z - I_y)\right] \tag{B23}$$

For the special case in which x, y, and z are principal axes of the vehicle, equation (B23) reduces to:

$$M_{x_G} = \frac{3K}{R^5} R_y R_z\ (I_z - I_y) \tag{B24}$$

Applying the above procedure to the y-axis, it can be shown that:

$$M_{y_G} = \frac{3K}{R^5}\left[(R_x{}^2 - R_z{}^2)\ I_{xz} + R_x R_z\ (I_x - I_z) + R_x R_y I_{yz} - R_y R_z I_{xz}\right] \tag{B25}$$

or, if the x, y, z-axes are principal axes, equation (B25) reduces to:

$$M_{y_G} = \frac{3K}{R^5} R_x R_z\ (I_x - I_z) \tag{B26}$$

Similarly, it can be shown that

$$M_{z_G} = \frac{3K}{R^5}\left[(R_y{}^2 - R_x{}^2)\ I_{xy} + R_x R_y\ (I_y - I_x) + R_y R_z I_{xz} - R_x R_z I_{yz}\right] \tag{B27}$$

or, if the x, y, z-axes are principal axes, equation (B27) reduces to:

$$M_{z_G} = \frac{3K}{R^5} R_x R_y \left(I_y - I_x\right) \tag{B28}$$

It should be remembered that the results obtained above are based on the assumption that the gravitational force generated by the attracting body on an element of mass in the vehicle is represented by equation (B1). The results are further limited by the validity of neglecting higher order terms in the binomial expansion used to obtain equation (B13).